The Arctic Sea Ice - Melting During Summer or not Freezing in Winter?

Henriette Bærheim Skaret

June 2016

A Thesis Presented for the Degree of
Master of Science in Climate Dynamics

Geophysical Institute
Faculty of Mathematics and Natural Sciences
University of Bergen

Acknowledgements

First of all, I would like to thank my supervisors **Tor Eldevik** and **Ingrid Husøy Onarheim** for your guidance and encouragement, as well as all of your helpful advice and comments regarding my thesis.

Additionally I would also like to give a special thanks to **Aleksi Nummelin** for providing me with the model data, and for your willingness to assist at all times with your programming expertise.

To my **fellow students**, particularly **Heidi**, **Helene** and **Kristine**, thank you for making the last five years absolutely unforgettable, you have been priceless to me.

And last but not least, I could not have written this thesis without the support and motivation that I have received from **my family**, **Sondre** and **his family**.

Henriette Bærheim Skaret
Bergen, 2016

Abstract

The Arctic sea ice cover has retreated rapidly during the last three decades, concurrent with recent global temperature increase both in the atmosphere and in the ocean. The sea ice cover has experienced a retreat in extent and a reduction in thickness, hence the sea ice volume is declining. As a consequence, the multi-year sea ice is decreasing, and first-year ice is now the dominating ice type in the Arctic Ocean.

This study uses the Norwegian Earth System Model (NorESM), forced at the surface with atmospheric reanalysis data from the Coordinated Ocean-ice Reference Experiments phase II (CORE-II), during the period from 1948 to 2007. The model simulation is compared to available observations, both from satellites and in-situ observations, for model evaluation. Since there are large regional and seasonal differences of the sea ice cover in the Arctic, this study provides an evaluation of the regional and seasonal variations in 12 different Arctic regions, where March represents the winter (maximum sea ice cover in the Northern Hemisphere) and September represents the summer season (minimum sea ice cover in the Northern Hemisphere). There are particularly two 20-year periods in the model simulation with noticeable trends in sea ice extent, Period I (1948-1967) and Period III (1988-2007), which are analyzed in more detail. The Barents Sea is in particular focus in this study, and the decreasing sea ice in this region is found to be associated with observed changes in temperature during these periods, both in the atmosphere and the ocean.

The model simulation shows significant negative trends over the last 20 years, and there has been a loss of sea ice in all Arctic regions in the winter season as well as the summer season. However, the sea ice declines regionally and seasonally at different rates. Seven of 12 regions in the interior Arctic Ocean have more or less a full sea ice cover in all winters, and these regions are thus only contributing to the summer sea ice extent trends in the Northern Hemisphere. It is suggested that the loss of sea ice in these regions is dominated by increased melting towards summer. Two of 12 regions located in the north of the Pacific are completely ice-free during summer, and the diminishing sea ice cover in these regions are hence suggested to be due to reduced freezing of sea ice towards winter. For the remaining three regions, and for the Northern Hemisphere in total, variations

are seen in all months of the year. The trends in Baffin Bay are greatest in winter, which indicates that the region is dominated by reduced freezing. For the Greenland Sea, the trends in March and September are on the same order of magnitude, and in the Barents Sea the trends in sea ice concentration and sea ice extent contradict each other. However, because these two latter regions approach ice-free conditions in the summer season, decreased winter freezing is seen in recent observations in the Barents Sea. As a result, decreased winter freezing will therefore likely be the dominating cause of sea ice loss in these regions in the model simulation for the years following 2007. For the Northern Hemisphere in total, the interannual variability and the long-term trend (both in sea ice concentration and in sea ice extent) are clearly greatest in the summer season, suggesting that the total loss of sea ice in the Northern Hemisphere is due to increased melting towards the summer.

Contents

List of Figures

List of Tables

Chapter 1

Introduction

Climate change is one of the main present human concerns, and will likely remain so for a long period ahead, due to the many risks it poses to both nature and societies. Observed consequences of climate change include increasing surface air temperatures, melting of sea ice and glaciers, rising sea levels and extinction of species (Hartmann et al., 2013). Changes in weather patterns will likely be a part of a changing climate, with increased incidents, intensity and duration of heat waves, drought, heavy precipitation and tropical cyclone activity (Stocker et al., 2013). The changing climate also has implications on food production, water supply and spread of diseases (Rosenzweig et al., 2001).

According to Hartmann et al. (2013), globally averaged land and ocean surface temperatures show a warming of 0.85°C over the period 1880-2012, calculated as a linear trend. How fast the global temperature will increase in the future will be a determining factor for the consequences of climate change. Anthropogenic emissions, e.g., from the burning of fossil fuels, are a major contribution to the increasing global temperature (IPCC, 2013). Human induced emissions must be limited in order to reduce and possibly control the magnitude of the consequences of global warming.

Global warming does not occur at the same rate on Earth, in fact the polar surface air temperature increases 2-3 times faster than the global-mean surface air temperature (e.g., Manabe and Wetherald, 1975; Serreze and Francis, 2006; Taylor et al., 2013). The amplification of surface air temperatures in the Arctic region is indicated in Figure 1.1. This phenomenon is known as polar amplification, and is likely caused by positive feedback mechanisms, along with changes in atmospheric and oceanic circulation (Førland et al., 2012). The surface albedo feedback is believed to be one of the main drivers of this amplification, and has great influence on the polar surface heat budget (Taylor et al., 2013). Albedo is a measure of how much shortwave solar radiation the planet reflects back to space. Snow and ice (with white surfaces) have a high albedo (close to one),

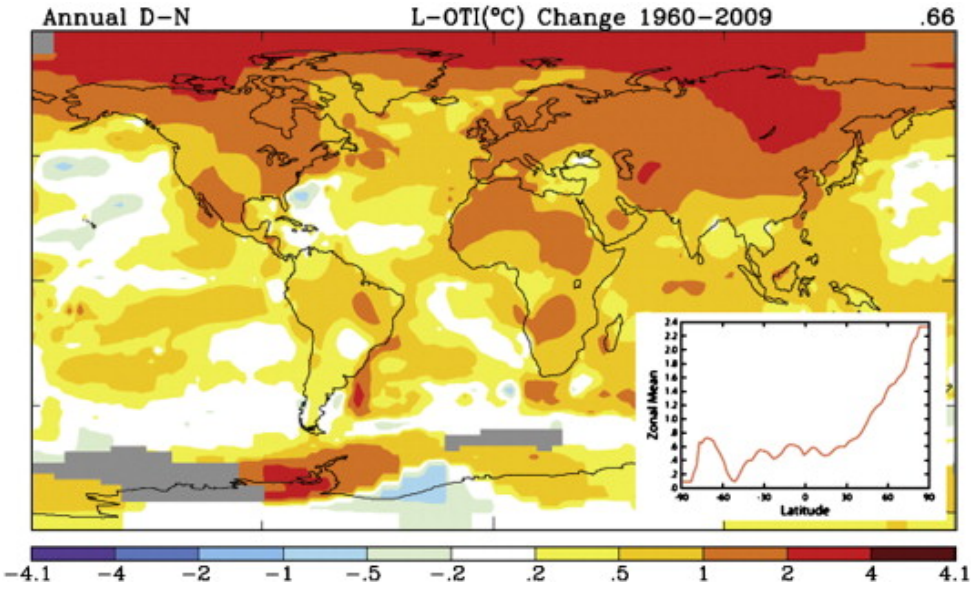

Figure 1.1: *Observed Arctic amplification. The figure is retrieved from Serreze and Barry (2011) and shows linear trends in annual mean surface air temperatures [°C] from the period 1960 to 2009 (calculated from December to November). The inset shows zonal mean linear trends for the 50-year period.*

meaning that they are efficient reflectors of solar energy. As a result of global warming, snow-covered land, sea ice and glaciers melts. A decrease in sea ice leads directly to more open water, reducing of the surface albedo and hence increasing the absorption of solar radiation. An accumulation of solar heat enables a transfer of more heat from the ocean to the atmosphere, which in turn may increase the atmospheric temperatures (Perovich et al., 2011). This positive feedback mechanism is called the ice-albedo feedback. Other feedbacks are also suggested as important temperature amplifiers in the polar regions, including cloud feedbacks and atmospheric dynamic transport (Taylor et al., 2013).

1.1 Arctic sea ice

One of the most prominent indicators of global warming is the observed changes in the Arctic sea ice cover over the last decades (see Figure 1.2). Ice and snow are sensitive to changes in air and ocean temperatures, as the sea ice responds to changes from both above (atmosphere) and below (ocean). As mentioned earlier, global warming has led to higher temperatures in both the atmosphere and the ocean, however the importance of higher temperatures differs on a regional basis. For instance, model results from Sandø et al. (2014) show that the ocean has a stronger direct impact on the melting and freezing of sea ice than the atmosphere near Arctic gateways. In fact, it has been observed a

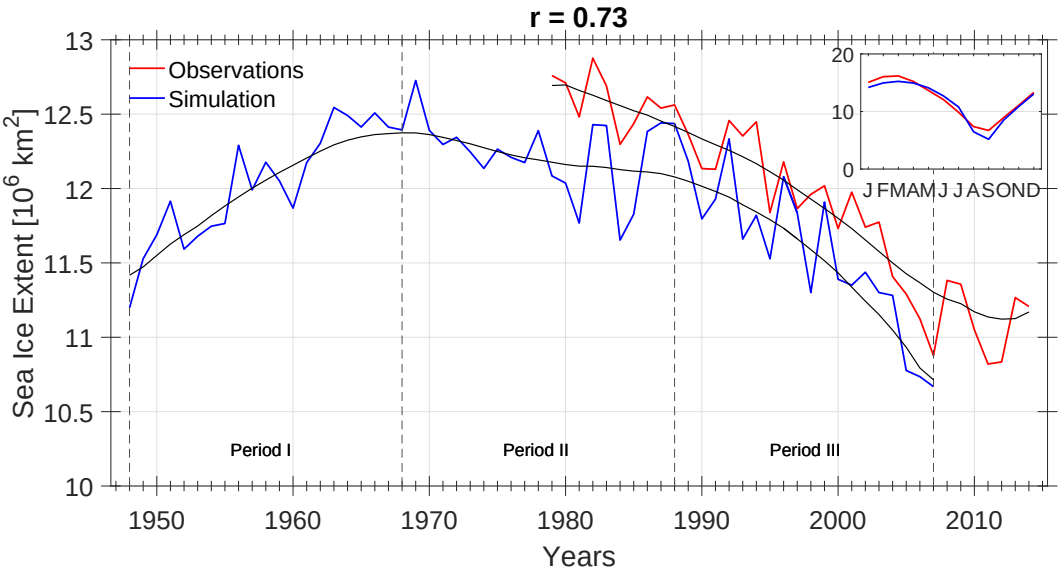

Figure 1.2: *Northern Hemisphere annual mean sea ice extent for the simulated data over the period 1948-2007 (blue), and observations from satellites over the period 1979-2014 (red), provided by the National Snow and Ice Data Center (NSIDC, Cavalieri et al., 1996). The black lines show the 11-year triangular smooth through each dataset (see Section 2.3.7 for details). The inset indicates the mean seasonal cycle (monthly mean) of sea ice extent from observations (red) and for the simulated data (blue), both averaged over the period 1979-2007. The correlation coefficient, r, between the two detrended data sets is also shown (for the period 1979-2007). The 60 years of model data are divided into three periods, Period I (1948-1967), Period II (1968-1987) and Period III (1988-2007), with two decades in each period.*

stronger advection of warmer water into the Arctic region recently, both through the Barents Sea Opening (Årthun et al., 2012) and the Bering Strait (Woodgate et al., 2006). This stronger and warmer inflow of water into the Arctic has consequences for the sea ice, especially in the Barents Sea where a reduction of nearly 50 % of annual mean sea ice area has been observed in the period 1998 to 2008 (Årthun et al., 2012). A reduction of sea ice extent (see Section 2.2.2 for definition) has occurred recently, and an ongoing thinning of the sea ice cover has also been observed (e.g., Rigor and Wallace, 2004; Haas et al., 2008). Additionally, there has been a regime shift from multi-year ice (ice that still remains after the summer minimum) to first-year ice, which largely explains the decline in sea ice volume and thickness (Kwok et al., 2009; Comiso, 2002). In fact, seasonal ice is now the dominant ice type in the Arctic. A thinner sea ice cover in the Arctic may lead to a more rapid decrease of sea ice, as thinner ice needs less heat in order to melt completely than thicker ice. Thinner ice is also more vulnerable and easier to move by, e.g., wind and ocean currents (Ivanov et al., 2016). A reduced sea ice cover as a result

of wind and ocean currents will not be in the scope of this study, but we note that these factors are important in the recent loss of Arctic sea ice.

The Arctic sea ice extent varies throughout the year, and typically has its minimum in September, with an average of about $6 \cdot 10^6$ km^2, and its maximum in March with an average of about $16 \cdot 10^6$ km^2 (calculated from satellite observations over the period 1979-2014). Although the Arctic sea ice extent in total has exhibited a significant decline over the last few decades, there are huge differences in the rate of change among different regions within the Arctic Ocean. The trends range from +7.3 % change per decade of sea ice extent in the Bering Sea, to -13.8 % change per decade of sea ice extent in the Gulf of St. Lawrence during the period from 1978 to 2012 (Vaughan et al., 2013). This large variability between different Arctic regions is believed to be closely related to the complexity of the atmospheric and oceanic circulation system, as well as their location. The interior of the Arctic Ocean is more isolated from incoming water from the south, while the regions located at the periphery of the Arctic are more vulnerable to changes in, e.g., the heat transport by ocean currents into the Arctic. The trends and ice coverage within each geographical region also vary from season to season, and changes in sea ice properties in each region largely depend on the seasonal cycle (Close et al., 2015). Since there has been a decrease of sea ice in the Arctic Ocean recently, it is crucial that we are able to understand and separate the differences between the current changes, previous changes and natural variability.

The evolution of the sea ice extent in the Northern Hemisphere can be seen in Figure 1.2. This figure shows observed and simulated yearly mean sea ice extent in the Northern Hemisphere in the period from 1948 to 2014. The simulation is from the Norwegian Earth System Model (NorESM) with the atmospheric forcing from the Coordinated Ocean-ice Reference Experiments phase II (CORE-II) from 1948 to 2007 (blue). The observations of sea ice from satellites can also be seen in the period from 1979 to 2014 (red). The data sources used in this thesis are described in more detail in Section 2.1. The model simulates the sea ice well in the period where observations are available, and shows that the sea ice extent increases from 1948 to 1979. The model simulation, which will be the main dataset in this study, is divided into three different 20-year periods, based on the long-term variations seen in the data. Period I (1948-1967) shows an overall increase in sea ice extent, Period II (1968-1987) shows a more stable sea ice extent (but yet a decrease), and Period III (1988-2007) shows a strong decline in sea ice extent. These periods will be used throughout this thesis, with most emphasis on Period I and Period III, due to the fact that the greatest changes in sea ice extent occur in these periods.

The sea ice extent has a clear negative trend during the last three decades, which is seen both in the model simulation and in the observations (indicated by the black lines in Figure 1.2). The trends are decreasing more or less with the same rate, however the trend in the model simulation is weaker than the trend in the observations during the period 1980-1990. Both time series show that there is large interannual variability in Arctic sea ice extent, and the time series are closely linked, indicated by the high correlation between the detrended time series ($r = 0.73$, see Section 2.3.2 for explanation). However, there is a noticeable difference in the amount of sea ice between the observations and the model, where the model simulates approximately $0.25 \cdot 10^6$ km^2 less sea ice than what is observed. The simulation used in this study underestimates the sea ice extent both for September and March compared to the observations (Figure 1.2). Wang et al. (2016) show that all model configurations that are based on the same sea ice model that is used in this study are prone to underestimate the sea ice extent, which suggests that the underestimation of the sea ice extent may be linked to the sea ice model.

The effects of the ongoing melting of snow and ice are many, both locally and globally. The local weather and climate in the Arctic Ocean and adjacent seas are effected by a decrease of Arctic sea ice (Vihma, 2014). For example, the Arctic wildlife will be affected by a warmer climate. The polar bear, for instance, uses the sea ice as a platform when hunting seals. Ice loss from glaciers can have a direct impact on water resources in populated areas. Loss of Arctic sea ice has altered, and may continue to alter, the ocean circulation and regional climate (Serreze et al., 2007). In addition, opening of the Arctic Ocean raises many important discussions regarding shipping, fishing and the exploration of oil and gas in the Arctic. Global effects of global warming also includes loss of ice from ice sheets, such as Greenland and Antarctica, which plays an important role on global ocean circulation. A melting of these large ice sheets results in rising sea levels.

1.2 Numerical models

Only a century ago, weather forecasting was based largely on empirical methods by individual meteorologists. At this time there was less knowledge about the atmosphere, in addition to a limited amount of meteorological data to use as initial conditions. There has been a significant progress in dynamical meteorology since then, and thus made it possible to make numerical weather forecasts. Eventually, the computer was also invented, which in turn truly improved the weather forecasting (Kimura, 2002).

A computer can deal with a huge amount of data and process current weather conditions all over the globe. It can also perform complicated mathematical and dynamical calcu-

lations, satisfying physical conservation principles at any given time. Such conservation principles could for instance be the conservation of mass, heat, momentum and moisture (Mason, 1986). Complex weather models of the atmosphere and the ocean can further be developed based on physical and dynamical laws, e.g., the Navier-Stokes equations in a rotating frame. Since the atmosphere and the ocean are dynamically connected to each other, a model of the atmosphere and a model of the ocean can be coupled to each other. However, solving all of the nonlinear differential equations in a system like this is not possible to do analytically, not even for a computer, and hence approximations and assumptions have to be made in the numerical models (Pielke, 2013). As a result of the numerical approximations, the models do not simulate the climate perfectly. The reduced complexity, as a result of the simplifications in the computation, is one of the reasons why future projections have uncertainties.

Despite their limitations and simplifications, model simulations are valuable in scientific research, as they are used to assist in understanding, simulating and predicting the dynamics of the climate system (Wang et al., 2016). In addition, by comparing different models with observations, or with other independent models, we get an improved understanding of our climate and its dynamics. This contributes to identify model improvements, allowing us to develop more complete and accurate climate models. Moreover, numerical models provide complete datasets, which compliments observed datasets, since they are generally limited in space and time. Numerical models can also provide simulations of the global climate in the period before observations from satellites are globally available (before 1979).

It is crucial that we acquire as much knowledge as we can about the physical processes in our climate system, and how these processes interact with each other, to be able to understand the ongoing changes. By doing so, we will be one step closer to developing (even) more reliable climate models, and also know how to interpret the output of these models in the most accurate manner.

1.3 This study

Due to the large regional sea ice variability in the Arctic Ocean (see Section 1.1), it is interesting to assess the sea ice on a regional basis. Hence, the Arctic Ocean is divided into different regions in this study, as shown in Figure 1.3. From Figure 1.2, it is evident that there are especially two interesting periods to analyze, Period I (1948-1967) and Period III (1988-2007), as the Northern Hemisphere has a rapid increase and decrease in sea ice extent in these periods, respectively. This thesis will thus assess the long-term variability

of the sea ice cover, as well as analyze the interannual variability of the sea ice extent. The spatial distribution of trends is shown and compared in both of these periods for the summer season as well as for the winter season, and for each Arctic region. Furthermore, the trends are compared to see in which Arctic regions the largest interannual variability occur, where the strongest trends are found and in which season the trends are largest.

The ocean and sea ice component of the Norwegian Earth System Model (NorESM), forced with the atmospheric reanalysis data from the Coordinated Ocean-ice Reference Experiments phase II (CORE-II), are used to investigate the sea ice cover in each of the Arctic regions during the period from January 1948 to December 2007. This simulated dataset is referred to as the model data in this study. Since the observational sea ice records started in 1979, the simulation contribute to understand the Arctic sea ice cover before the instrumental observations began, as the simulation goes back to 1948. However, observational data will also be introduced in addition to the model data in parts of this thesis to evaluate the model simulation, and to show possible differences between observed and simulated Arctic sea ice.

This thesis is organized as follows; Chapter 2 gives a more detailed description of the data that is used in this thesis, the methods used to process the data and definitions of central statistical methods. The results are presented in Chapter 3, and a discussion based on central findings are given in Chapter 4. Finally, concluding remarks are found in Chapter 5.

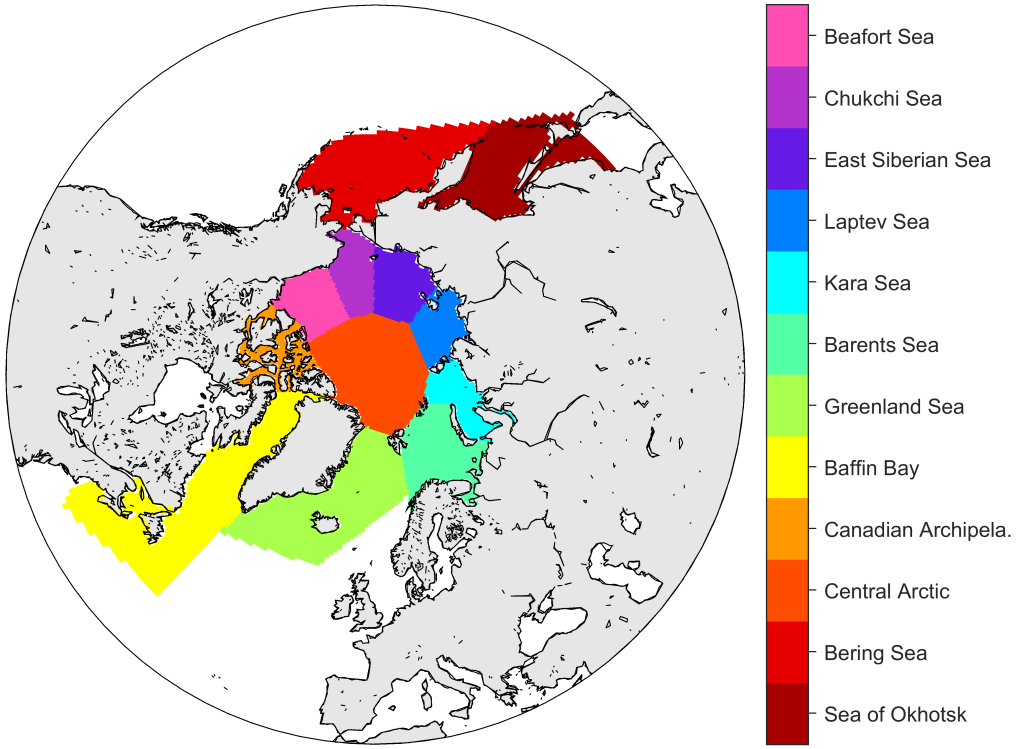

Figure 1.3: *Map of the Arctic Ocean, including the 12 Arctic regions used in this study. Region coordinates are obtained from Fetterer et al. (2010).*

Chapter 2

Data and Methods

This chapter is divided into three parts; (1) the two main data sources used in this thesis are described, (2) the methods for the processing of these datasets are explained and (3) statistical methods that are used in this study are presented.

2.1 Datasets

There are two main data sources used in this study, one containing a model simulation and one with observational data. These data sources are described in more detail in this section, including how the data has been produced and the properties of the datasets.

2.1.1 Model data

In this study we use results from hindcast simulations, with the ocean and sea ice components of the Norwegian Earth System Model (NorESM), forced with the atmospheric reanalysis from the Coordinated Ocean-ice Reference Experiments phase II (CORE-II) at the surface. Only the ocean components of NorESM (NorESM-O) is used in this study, which originates from MICOM (see Bleck and Smith, 1990). The sea ice model is based on the Los Alamos sea ice model, version 4 (CICE4, see Hunke et al., 2010). For a more detailed description of the NorESM configuration, see Bentsen et al. (2012).

The Coordinated Ocean-ice Reference Experiments (COREs) were suggested by the CLIVAR Working Group on Ocean Model Development to compare global ocean-sea ice models using a common interannually varying atmospheric forcing over the 60-year period from 1948 to 2007 (the atmospheric state is described in Large and Yeager, 2009), following the CORE-II protocol first described in Griffies et al. (2014). All models in the project are run for 5 consecutive loops of the 60-year forcing period (300 years). The CORE-II simulations are usually referred to as hindcast experiments in the oceanographic

community, and the CORE-II experiments directly contribute to evaluation, understanding and improvement of the ocean components in earth system models (Danabasoglu et al., 2014).

A larger model intercomparison project is presented in Wang et al. (2016) and Ilicak et al. (2016), consisting of fourteen models that simulate the Arctic region in the framework of CORE-II. A similar study is also done for the North Atlantic by Danabasoglu et al. (2014), which consists of two parts (mean state and variability analysis). NorESM is participating in these CORE-II projects.

The model data used in this thesis consists of monthly mean global sea ice concentration and sea surface temperature (no leap years), and contains data in the period from January 1948 to December 2007 (60 years), with a spatial resolution of $1^\circ \times 1^\circ$. The monthly mean values are further used to find annual mean values and the seasonal cycle of the sea ice cover. The sea ice concentration from the dataset is further used to derive the sea ice extent, which is described in Section 2.2.2.

2.1.2 Observational data

As a supplement to the model data, which is the focus of this thesis, observational data is used for comparison. The sea ice observations are obtained from the National Snow and Ice Data Center (NSIDC) and consists of passive microwave data of sea ice concentration, derived from brightness temperature data from satellites (Cavalieri et al., 1996). The data is gathered from the platforms Nimbus-7 and DMSP (Defense Meteorological Satellite Program) with the sensors SMMR (Scanning Multichannel Microwave Radiometer), SSM/I (Special Sensor Microwave/Imager) and SSMIS (Special Sensor Microwave Imager/Sounder). The dataset comes in a polar stereographic projection with a spatial resolution of 25×25 km, and it consists of monthly mean values from the 36-year period from January 1979 to December 2014. A common problem when dealing with observations from satellites is the lack of data in a circular sector around the North Pole, due to the orbit inclination of the satellite. A description of how this is handled will be given in problematic situations. Note that the model simulation used in this thesis has no data gaps.

2.2 Processing the data

There are different ways to describe and quantify the sea ice cover, including sea ice concentration, sea ice extent and sea ice area (defined below). Each of these measures have

their advantages and disadvantages. As they provide slightly different information, the measure of sea ice that is used will therefore differ from one situation to another, depending on the most relevant measure in each particular situation. The sea ice concentration and the sea ice extent are the the main measures used in this study.

2.2.1 Sea ice concentration

Climate models represent the Earth with grid cells, and each grid cell in a climate model contains information about the sea ice. This information is compiled in a measure called sea ice concentration. Sea ice concentration is a unitless term that describes the relative amount of sea ice in a grid cell, compared to the size of the grid cell itself. In other words, it contains information of the fracture of sea ice in the grid cell, and in this thesis it will be given as a percentage (0 % is ice-free, 100 % is completely ice-covered). The lack of observational data in the areas around the North Pole is simply treated as 100 % sea ice concentration, as the central Arctic Ocean is generally ice covered.

2.2.2 Sea ice extent

Sea ice concentration is used to derive the measure sea ice extent. Sea ice extent is a common way to measure changes in the sea ice cover (e.g., Parkinson and Cavalieri, 2008). If a grid cell contains 15 % sea ice concentration or more (15 % sea ice represents the sea ice edge), the cell is defined to be 100 % ice covered. If the grid cell contains less than 15 % sea ice, the grid cell is considered to be ice-free and is treated as 0 % sea ice. By multiplying each of the grid cells that contains over 15 % sea ice concentration with the area of the grid cell, and then sum all of these areas up, the sea ice extent is found (Parkinson and Cavalieri, 2008). In other words, the sea ice extent is the cumulative area of all ice covered areas ($\geq$ 15 % sea ice). The areas around the North Pole are treated as completely ice-covered (100 % ice) in the observational data, meaning that the grid cell is interpreted to contain sea ice concentrations above 15 % in the definition of sea ice extent, which is a reasonable assumption (Parkinson and Cavalieri, 2008).

2.2.3 Sea ice area

Sea ice area is another way of measuring the sea ice cover. Like the sea ice extent, sea ice area is also based on the threshold of 15 % sea ice concentration, and all grid cells with sea ice concentrations below 15 % will be considered ice-free. Sea ice area is defined as the product of the fraction of each grid cell's sea ice concentration multiplied with its respective area, and the total sea ice area is found by the sum of all of these areas (Parkinson and Cavalieri, 2008). Hence, the sea ice area expresses a more realistic value

of the true ice covered area on the ground compared to the sea ice extent. However, the satellite sensors are sensitive to surface melt and melt ponds on top of the ice, and will treat them as open water. Hence, in the melting season and during summer there could be some concern about using sea ice area, and the sea ice area is prone to underestimate the sea ice cover (Overland and Wang, 2007). This thesis will analyze the sea ice cover in the melting period, and therefore the measure sea ice extent will be used instead of sea ice area. The sea ice area is always smaller (or equal, if the sea ice concentration equals 100 %) than the sea ice extent (Cavalieri and Parkinson, 2012). The areas around the North Pole in the observational data are interpreted as areas with 100 % sea ice concentration, which is not very realistic at any time of the year.

2.3 Statistics

In order to draw conclusions from the results obtained in this thesis it is advantageous to have statistical concepts, and also set a threshold for when the result can be said to be statistically significant. This section will therefore describe essential statistical methods that are used throughout this study.

2.3.1 Mean, variance and standard deviation

The mean of a random variable, x, is defined as,

$$\bar{x} = \frac{1}{n}\sum_{i=1}^{n} x_i, \tag{2.1}$$

where n is the number of all data points, and x_i is each value of the data set. The variance is the average of the squared distance from the mean value $\bar{x}$,

$$s^2 = \frac{1}{n-1}\sum_{i=1}^{n} (x_i - \bar{x})^2. \tag{2.2}$$

The *sample standard deviation*, s, is the square-root of the sample variance, and is a measure of how dispersed the data is from the sample mean. It describes an average distance of the values $x_1, x_2..., x_n$ from the mean $\bar{x}$ (Hogg et al., 2014).

2.3.2 Covariance and correlation

The *covariance* between two datasets is a measure of the strength of interdependence between them, and is found by,

$$cov(x, y) = \frac{1}{n-1} \sum_{i=1}^{n} (x_i - \bar{x})(y_i - \bar{y}). \tag{2.3}$$

The covariance can be any real number, and has the same unit as the product between x and y. Note that the dependence of the variables is difficult to interpret by simply looking at the value of the covariance. Hence, a standardized version of covariance is used for this purpose, and is commonly known as the *correlation coefficient*, $r_{x,y}$. The correlation coefficient ranges from -1 to 1, where $r = -1$ means total anti-correlation (i.e., when one variable increases, the other variable decreases), $r = 0$ means no correlation and $r = 1$ means perfect correlation (i.e., when one variable increases, the other variable increases). The correlation coefficient is calculated by the following equation,

$$r_{x,y} = \frac{cov(x, y)}{s_x s_y}. \tag{2.4}$$

When the correlation coefficient between two data sets is close to ± 1, the data sets are strongly linked to each other statistically.

The statistic *variance explained* is based on the correlation coefficient, and is simply defined as $r^2_{x,y}$. It describes how much of the variance in variable, x, that is described, or predicted, by variable y.

2.3.3 Confidence intervals

In this study it is assumed that the data we are working with is normally distributed around the population mean, μ. This is often a good assumption in statistics, due to the *central limit theorem*. A simplified explanation of this theorem, is that when the sample is large enough, the distribution of sample means $\bar{x}$ approaches a normal distribution. However, the population mean is generally not a known variable. Thus, μ is estimated by the sample mean, $\bar{x}$.

A *confidence interval* is an interval that has a specific probability of including the real value of the parameter, μ. This probability is equal to $1 - \alpha$, where α is the significance level. A significance level has to be chosen to know when the result can be said to be statistically significant, and a common choice is the significance level 5 %, $\alpha = 0.05$. This significance level will be used in this thesis, unless otherwise stated. In a normal distribution, 95 % of the data lies within 1.96 standard deviations from the mean. By choosing this significance level, we accept a 5 % chance of doing a rejection error, and this indicates the probability that the observed difference between the datasets is due to chance (Bjørnstad, 2009). The probability density function becomes concentrated around

an interval, with its center in the point estimate, $\bar{x}$. The equation for the confidence interval for the mean is,

$$\left[\bar{x} - t_{\alpha/2}(n-1)\left(\frac{s}{\sqrt{n}}\right), \bar{x} + t_{\alpha/2}(n-1)\left(\frac{s}{\sqrt{n}}\right)\right], \tag{2.5}$$

where n is the sample size, s is the sample standard deviation and $t_{\alpha/2}(n-1) = t_{0.025}(n-1)$ (this number can be found in a statistical table). Note that if the sample size, n, increases, the term $t_{\alpha/2}\left(\frac{s}{\sqrt{n}}\right)$ decreases, resulting in a shorter confidence interval and hence a higher credibility in $\bar{x}$ as an estimator of μ (Hogg and Tanis, 2010).

2.3.4 P-value

The *p-value*, or the *probability value*, is the probability that the test statistic is equal to, or exceeds, the observed value of the test statistic. Note that if the p-value is smaller than the significance level, α, the result is said to be *statistically significant*. The smaller the p-value is, the larger the significance and the more certain you can be that the differences are not due to chance.

P-values are used in this thesis when testing the significance of the correlation coefficients. The hypothesis that there is no relationship between the two time series is tested, and p-values are calculated to test for a significant correlation, where $p < 0.05$ shows significance on the 5 % level. Linear trends are also tested to see if they are significant, and the *F-test* is used to test for a significant linear regression relationship. This is performed by calculating the p-value from the F-statistic.

2.3.5 Degrees of freedom

Degrees of freedom is, in statistics, the number of dimensions in which a random vector is free to vary, and is equal to the difference between the number of variables and the number of parameters in the statistical model (Bjørnstad, 2009). In other words, it is the number of independent ways a system can move. However, the number of free parameters is rarely defined. Therefore, the degrees of freedom often has to be approximated, and are thus called *effective degrees of freedom* (Janson et al., 2015). The effective degrees of freedom for observations are found from the following equation,

$$n_{eff} = \frac{n}{1 + 2(r_1 r_1' + r_2 r_2' + ... + r_n r_n')}, \tag{2.6}$$

where n is the sample size in the data set, r_1 and r_1' are the lag-1 autocorrelations of two time series, r_2 and r_2' are the lag-2 autocorrelations, continuing up to the n'th value

(Quenouille et al., 1952).

However, in this thesis, the auto-correlation has not been accounted for in statistical computations. We therefore note that the statistical significance in this thesis might be too optimistic.

2.3.6 Trends

Trend lines are often used to describe the behavior of the data over a given period of time, and relates the data to the time it occurred. A trend line can have many shapes, for instance linear, polynomial etc. Changes in climate do not necessarily happen linearly, however, linear trends are used in this thesis over periods where the trends are relatively close to linear (Figure 1.2).

To calculate a linear trend line, it is assumed that you have n data points which can be modeled by a first-degree polynomial (Montgomery et al., 2015). This simple linear regression equation is given by,

$$y = \alpha + \beta x, \tag{2.7}$$

where α is the intercept, β is the slope and x is the variable. The method of linear least-squares aims to minimize the summed square between the data points y_i and the modeled line, y. The unknown coefficients, α and β, are found by minimizing the equation $S(\alpha, \beta)$,

$$S(\alpha, \beta) = \sum_{i=1}^{n} (y_i - \alpha - \beta x_i)^2. \tag{2.8}$$

This equation is minimized by differentiation the equation with respect to each of the parameters, α and β, and setting the result equal to zero (this calculation will not be explained in further detail in this study).

2.3.7 Smoothing and filtering

Time smoothing is widely used in geophysical problems, e.g., the calculation of monthly mean, yearly mean and decadal mean values (Holloway, 1958). The underlying trend and seasonal components can also be found more clearly by filtering. Smoothing a time series can be done by, e.g., removing high frequencies, which are often assumed to be noise, random variations, aliasing or insignificant values with respect to the evaluation. A smoothing like this will therefore make sure that the short-term variations are attenuated and the long-term variations appear more clearly. This is called a *low-pass filter*. On the other hand, the *high-pass filter* only allows the high frequency components to pass,

while the low frequency components are attenuated. The process of smoothing a time series is done by mathematical functions, which generally consists of fractional values called *weights*. The time series are then cumulatively multiplied by these weights. The weights can (for instance) be cumulatively cross-multiplied by adjacent values in the time series, and this process is performed from the beginning till the end of the time series. An example of the simple 3-point moving average is calculated by the following equation,

$$S_i = \frac{Y_{i-1} + Y_i + Y_{i+1}}{3}, \tag{2.9}$$

where S is the signal undergoing the smoothing and Y_i are the data points in S. This moving average is calculated from the second data point to the second last data point in the signal, as this calculation is not possible in the endpoints.

Smoothing of a time series is best performed with an odd numbered width, since the coefficients then are balanced symmetrically around the central point.

A filter that is widely used in this thesis is the triangular moving average, as this filter is a better low-pass filter than, e.g., the simple moving average. The simple moving average still showed fluctuations on a decadal timescale, while the triangular filter managed to remove more or less all the short-term changes in the 11-year window. This thesis uses filters only to illustrate and point out long-term changes, allowing the elements at the edges (the first 5 years and the last 5 years in the time series) to be reduced in the calculation, so that the actual window size at the edges is less than the specified 11-year window. To illustrate how the triangular moving average function looks like, a 5-point triangular window is calculated as follows,

$$S_i = \frac{Y_{i-2} + 2Y_{i-1} + 3Y_i + 2Y_{i+1} + Y_{i+2}}{9}, \tag{2.10}$$

where S is the signal undergoing the smoothing, Y_i are the data points, the coefficients are the *weights* and the denominator is the sum of the coefficients in the numerator (O'Haver, 1997). This filter smooths the time series using a recursive algorithm, and is equivalent to two passes of a 3-point sliding rectangular filter.

High-pass filters are also used in this study. When a time series is detrended, the long-term variations (the least-square trend line, see Section 2.3.6) is removed from the time series, so that only the short-term fluctuations remain. Detrending of the data is done before calculating the correlation coefficient between two datasets, so that only the short-term variations are compared.

Chapter 3

Results

In this chapter, the results obtained from the model simulation are presented in various ways for the Northern Hemisphere, and particularly for the 12 different Arctic regions shown in Figure 1.3. Variations in sea ice concentration in the Northern Hemisphere are illustrated as monthly snapshots, giving a brief overview of where the sea ice cover is located in the Arctic Ocean in March and September for different years. Temporal variations are shown as annual mean time series to see how the interannual variations unfold in each of the defined Arctic regions, and later the seasonal cycle is presented both for the Northern Hemisphere in total, and for the different Arctic regions. Trends are calculated in March and September for each of the Arctic regions, both for the sea ice extent and for the sea ice concentration. Finally, the spatial anomalies (calculated from the the mean period from 1948 to 2007) are shown for the year with the smallest sea ice extent in the model simulation (2007).

3.1 Northern Hemisphere sea ice concentration

Figure 3.1 shows maps of the sea ice concentration in 1948, 1979 and 2007 for March and September. It is interesting to see if there are any substantial temporal and regional differences in the loss of sea ice between the summer season with minimum sea ice extent and the winter season with maximum sea ice extent. The figure is consistent with the model simulation in Figure 1.2, as the sea ice cover increases from 1948 to the 1970s, and then decreases from the 1970s to 2007, where it reaches its lowest values. From Figure 3.1, we observe that the variations between the March sea ice concentrations are smaller than the variations seen between the September sea ice concentrations. It is also worth noting that the changes in the location of the sea ice cover occur in different regions in the Arctic in the summer season and in the winter season.

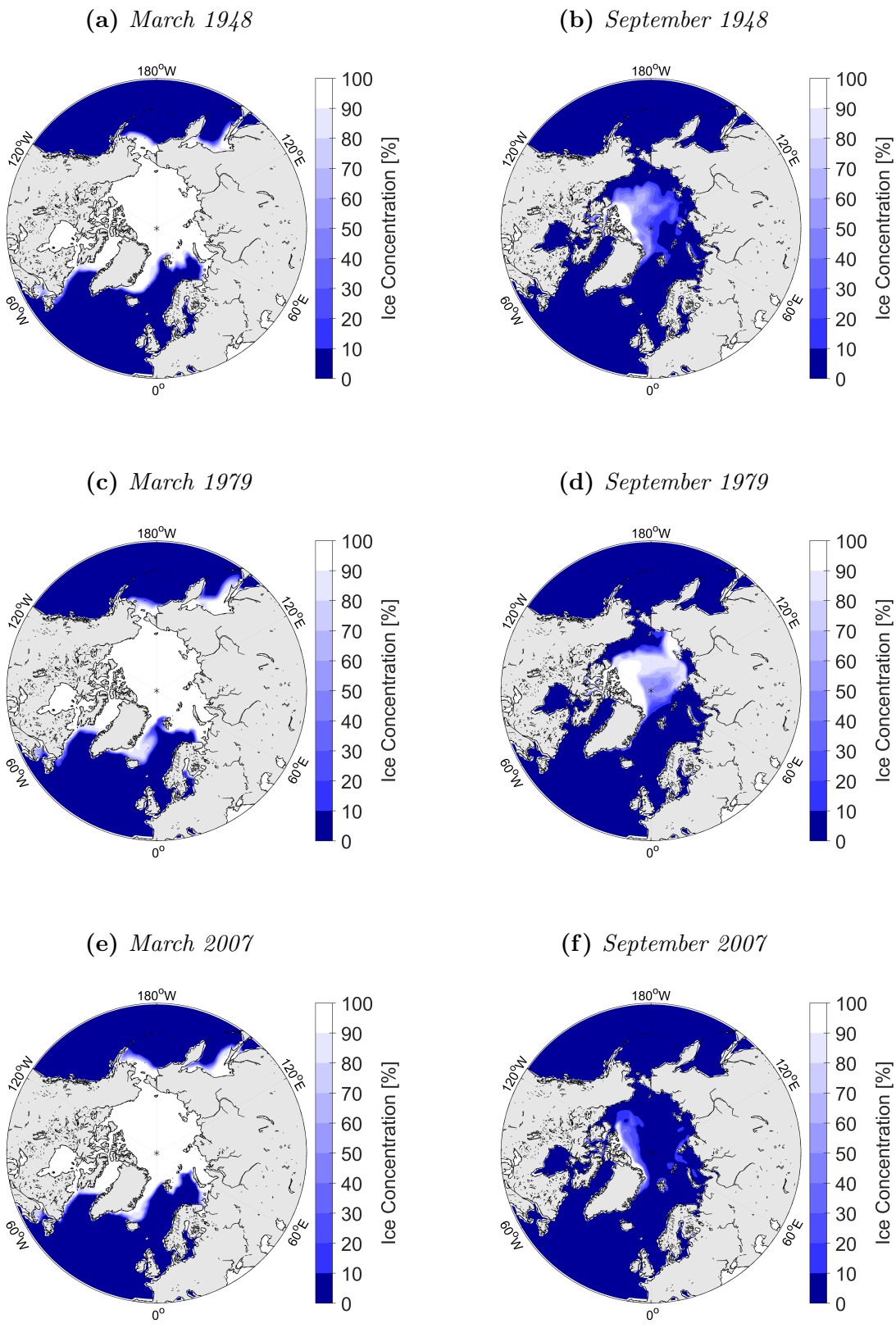

Figure 3.1: *Northern Hemisphere sea ice concentration with March values in the left column and September values in the right column for the three years 1948, 1979 and 2007, respectively.*

From Figure 3.1 it appears that the greatest changes in sea ice concentration in March occur in the Barents Sea, Greenland Sea, Bering Sea and Sea of Okhotsk, which are the outermost regions in the Arctic (see Figure 1.3 for regional definitions). However, this figure only shows monthly snapshots of the sea ice concentration in three given years, and the changes in this figure are not necessarily the long-term trend of sea ice concentration, since the sea ice edge is constantly changing due to changes both in the atmosphere and in the ocean. Nevertheless, in this case, it represents the long-term trend, since these years are selected specifically out of the long-term trends as seen in Figure 1.2. Later in this chapter, a spatial distribution of trends in sea ice extent are shown in Table 3.2, and also the spatial distribution of long-term trends in sea ice concentration is shown in Figure 3.5.

Since March is the month with the largest sea ice extent, almost all of the central parts in the Arctic Ocean are completely ice-covered. The marginal regions are mostly ice-free in September, hence the regional changes in September occur in different regions than seen in March. For the sea ice concentration in September, the sea ice is mostly located in the western Arctic Ocean for all of the three years (i.e. close to Greenland and the Canadian Archipelago), while the eastern side of the Arctic Ocean (i.e. close to Russia) is mostly ice-free. However, when the sea ice concentration increases from 1948 to 1979 (e.g., Figure 1.2), the sea ice concentration in Figure 3.1 increases in the Central Arctic and also in the eastern Arctic Ocean, such as in the Laptev Sea and in the East Siberian Sea. When the sea ice cover again retreats towards 2007, the sea ice retreats from this side of the Arctic Ocean, and is now located only in the western Arctic Ocean, close to the land areas around Greenland, which is also the case for 1948.

3.2 Regional and annual sea ice variability

Figure 3.2 shows the annual mean sea ice extent for all of the 12 Arctic regions in this study (see Figure 1.3) from 1948 to 2007, with a red 11-year moving mean triangular filter running through the time series to illustrate decadal changes (see Section 2.3.7 for more details about filtering). Figure 3.2 is divided in the same three 20-year periods as the time series for the whole Northern Hemisphere (Figure 1.2). The vertical axis has a range of $0.6 \cdot 10^6$ km^2 for all areas, but the values on the axes vary from panel to panel. Since the range is the same for all figures, it is possible to compare interannual variations and long-term trends in different regions, and it will be clearer which areas have the steepest trend and the greatest interannual variations. We note that many regions have large interannual variability, while other regions have less interannual variability. However,

the decadal mean (red line), and thus the long-term variation, is used as a basis for the description in this section.

The time series of the model data for the entire Northern Hemisphere (Figure 1.2) shows that the sea ice extent is increasing from 1948 to 1967 (Period I), the sea ice cover stays relatively stable (with a slight decrease) from 1968 to 1987 (Period II), before it decreases to its absolute minimum from 1988 towards 2007 (Period III). The same pattern is seen fully or partly in many of the study regions, which is not surprising since all the regions combined make up Figure 1.2. The typical pattern for the Northern Hemisphere is most apparent in f) Barents Sea, g) Greenland Sea and j) Central Arctic. These regions experience an increase in sea ice extent in Period I, followed by a slight decrease in sea ice extent with a relatively flat trend in Period II, before the area experiences a drop in sea ice extent in Period III. f) Barents Sea and g) Greenland Sea have a much greater drop after its main peak after Period I than the pattern for the entire Northern Hemisphere, which only experiences a relatively small sea ice loss, while j) Central Arctic has a smaller trend in Period II than the Northern Hemisphere. j) Central Arctic seems to be almost completely ice-covered in Period II, as the interannual variations are small and the trend in this period is very stable.

Other regions also show the main pattern, however these are less clear because of the smaller variations than the areas already mentioned. a) Beaufort Sea, b) Chukchi Sea and e) Kara Sea have a slight increase in sea ice extent in Period I before the value decreases a little in Period II, followed by a further decrease in Period III. c) East Siberian Sea, h) Baffin Bay and l) Sea of Okhotsk increase until the middle and the end of Period II, before the sea ice extent decreases in Period III. The same happens in k) Bering Sea, except for the fact that the sea ice extent in Period III is fairly stable. d) Laptev Sea and i) Canadian Archipelago have a relatively stable ice cover in Period I and II, before the sea ice extent decreases slightly in Period III.

By calculating the correlation coefficient between the Northern Hemisphere and each different Arctic region, the variance explained can be found (see Section 2.3.2). Table 3.1 shows that the Central Arctic is the region that best explains the variance in the annual mean time series for the entire Northern Hemisphere (both for the original time series and when the time series have been high-pass filtered), with an explained variance of 36 % when the time series have been high-pass filtered (72 % for the original time series). The time series have been detrended with the 11-year moving mean for each region, shown in Figure 3.2. The Central Arctic is also the region with the greatest sea ice extent, and clearly has the greatest loss in sea ice extent in square kilometers (see Figure 3.2).

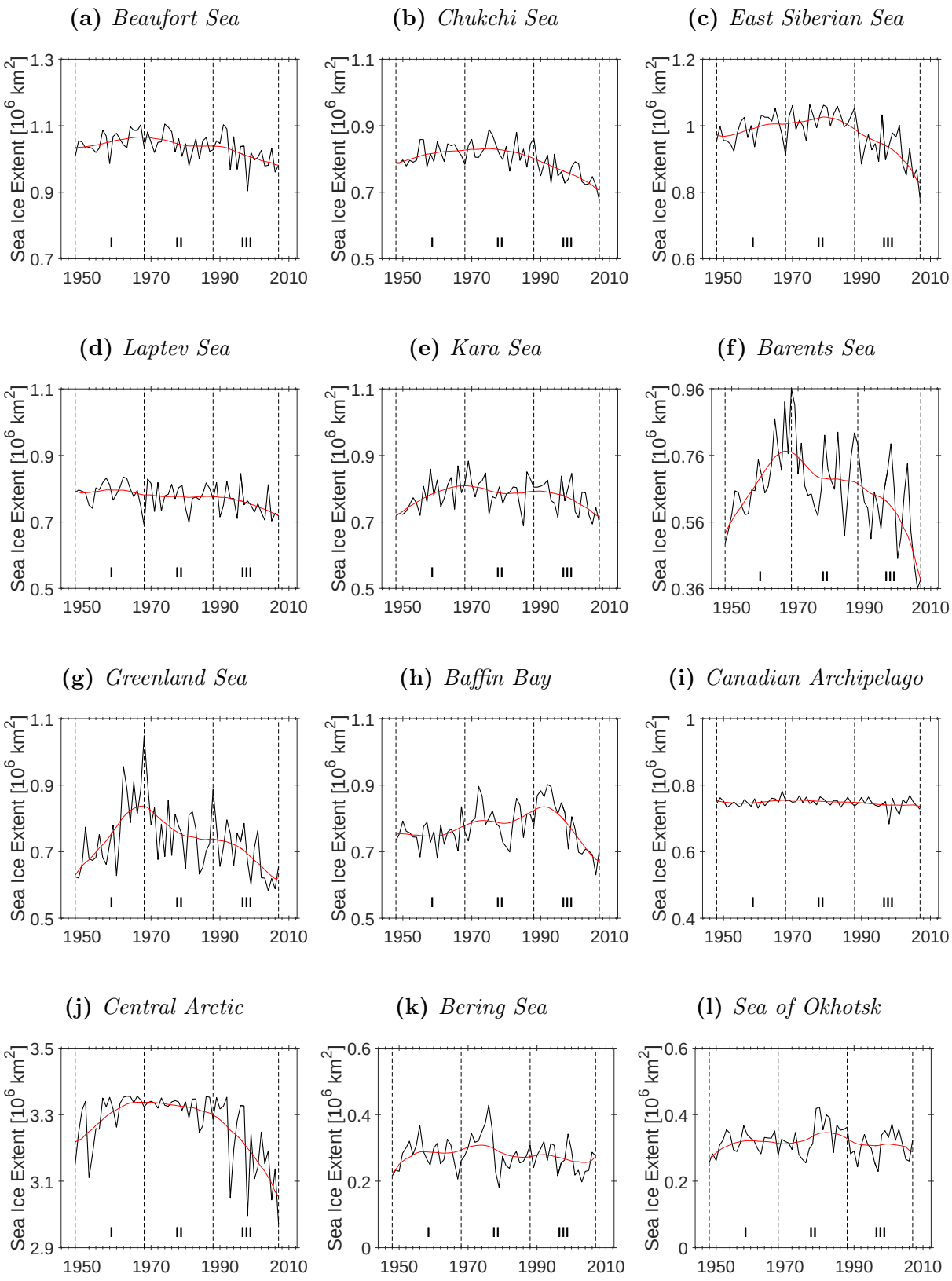

Figure 3.2: *Yearly mean sea ice extent for different regions in the Arctic (1948-2007). Note that the vertical axes are differing from region to region, but the range is the same. The red line is the 11-year running mean (triangular filter, see Section 2.3.7).*

When the time series are detrended, the Kara Sea is the region accounting for most of the variance in the Northern Hemisphere (after the Central Arctic), while the Barents Sea accounts for most of the variance (after the Central Arctic) when the time series are not detrended. Note that there is a great co-variability between the different regions, and that these values are a yearly mean. The correlations between the different regions and the Northern Hemisphere were also calculated for March and September (not shown) for the detrended timeseries (detrended with the 11-year moving mean). The marginal seas accounted for most of the variance in March, and the strongest correlation with the Northern Hemisphere was found in the Greenland Sea, the Barents Sea and the Sea of Okhotsk, respectively. In September, on the other hand, the Central Arctic dominated the explained variance, closely followed by the regions close to the Eurasian basin, namely the Chukchi Sea, the Laptev Sea and the East Siberian Sea.

The fact that f) Barents Sea, g) Greenland Sea and j) Central Arctic best reflects the pattern for the Northern Hemisphere as a whole (as seen in Figure 1.2), suggests that these three regions account for a lot of the variation seen for the Northern Hemisphere in total. For the original time series, the Central Arctic and the Barents Sea best describes the variance in the Northern Hemisphere. However, when the time series are detrended, the Central Arctic, the Kara Sea and the Laptev Sea explain the variance best. The magnitude of the correlation coefficients is in general reduced when the time series have been detrended. This fact suggests that the regions have more or less a common long-term trend, and that the interannual variations are different from one region to another.

The interannual and decadal variability vary between the different regions. The areas with the greatest interannual variability are typically not completely ice-covered during winter or completely ice-free during summer, allowing the interannual variations to be greater by increasing the months with variability, except from the Central Arctic (Figure 3.4j). The regions with largest interannual variability (indicated by the standard deviation in Table 3.1) are f) Barents Sea, g) Greenland Sea and j) Central Arctic, which are also the three areas with the greatest decadal variability. However, note that all regions are of different sizes and that the variability does not show how they vary compared to their own size or their mean sea ice extent, in other words the percentage of the increase/decrease of sea ice extent in the respective study region. In Table 3.2 the changes in sea ice extent with respect to the mean sea ice extent in each Arctic region is shown in % change per decade.

The region with absolutely smallest interannual variability and relatively stable values throughout the dataset, is i) Canadian Archipelago. i) Canadian Archipelago also has

the lowest standard deviation of all Arctic regions in the study period (Table 3.1). i) Canadian Archipelago is not the region with the smallest sea ice extent of the regions, so the small internannual variability is not because of the fact that this region has a lesser sea ice extent compared to other regions (since all regions are plotted with the same range). An explanation for this low variability can be explained by the seasonal cycle for the region, as seen in Figure 3.4i). As shown in this figure, i) Canadian Archipelago is completely ice-covered from November to June, and variations occur only four months a year. Out of these four months it appears that only three of them experience variability of a relatively large magnitude (August to October).

Table 3.1: *The correlation coefficients, r (original time series) and r_d (high-pass filtered with the 11-year moving mean indicated in Figure 3.2 for each region), and the variance explained, r^2 (not detrended) and r_d^2 (detrended), between the annual mean time series for the Northern Hemisphere and each Arctic region, in the period from 1948 to 2007. Note that the first and last five years have been cut out of each time series due to the limitations of the filter in the endpoints in the 11-year moving mean. The standard deviation, s_d, is calculated for each region after the time series has been detrended with the 11-year moving mean.*

	Beau.	**Chuk.**	**East**	**Lapt.**	**Kara**	**Bare.**	**Gree.**	**Baff.**	**Cana.**	**Cent.**	**Beri.**	**Okho.**
r	**0.61**	**0.72**	**0.74**	**0.50**	**0.64**	**0.75**	**0.66**	**0.43**	**0.42**	**0.85**	**0.26**	0.17
r_d	**0.40**	**0.36**	**0.41**	**0.49**	**0.53**	**0.45**	**0.30**	0.23	**0.43**	**0.60**	0.02	0.02
r^2	**37** %	**52** %	**55** %	**25** %	**41** %	**56** %	**44** %	**18** %	**18** %	**72** %	**7** %	3 %
r_d^2	**16** %	**13** %	**17** %	**24** %	**28** %	**20** %	**9** %	5 %	**18** %	**36** %	0 %	0 %
s_d $[10^6 \mathrm{km}^2]$	0.03	0.03	0.04	0.03	0.04	0.09	0.07	0.04	0.01	0.06	0.04	0.04

Beau. is Beaufort Sea, Chuk. is Chukchi Sea, East is East Siberian Sea, Lapt. is Laptev Sea, Kara is Kara Sea, Bare. is Barents Sea, Gree. is Greenland Sea, Baff. is Baffin Bay, Cana. is Canadian Archipelago, Cent. is Central Arctic, Beri. is Bering Sea and Okho. is Sea of Okhotsk

3.3 Seasonal cycles of sea ice extent

3.3.1 Northern Hemisphere

Figure 3.3a shows the seasonal cycle for the sea ice extent in the Northern Hemisphere for each year in the period from 1948 to 2007, where the values on the vertical axis are the monthly mean sea ice extent in each respective year. The data is grouped in six decades, where each decade contains ten seasonal cycles that are displayed with the same shade of color, where shades of red represent the initial years in this study going towards yellow colors for more recent years. The thick black line shows the mean seasonal cycle for the Northern Hemisphere over the entire study period.

The shape of the seasonal cycle is generally the same for all years, it has more or less a sinusoidal shape, with minimum sea ice extent in September and maximum sea ice extent in March. The first six months look like a smooth sine wave, while the months from July to December have more abrupt changes. The greatest change from one month to another is the loss of sea ice between July and August, where the sea ice is in the late melting process towards summer and its minimum extent.

The seasonal cycle for early years (red lines) are located both above and below the mean seasonal cycle (black line), and the sea ice extent is thus not consistently changing towards lower values over the 60-year period. Instead the seasonal cycle in Figure 3.3a shows the same pattern as the model data in Figure 1.2, where the sea ice extent first increases over a period, followed by a stable period, and then the sea ice extent decreases to an even lower value. However, it is clear that the yellow lines (recent years) are lower than any of the red lines, indicating that the total sea ice extent has been decreasing with time, and in each month of the year.

Figure 3.3b shows the associated boxplot of the seasonal cycle discussed above, with the median, 25th and 75th percentiles and the range. The boxplot, together with additional information from the color change in the seasonal cycle, clearly shows that most of the variability and the largest trend occur in the late melting season and in the beginning of the freezing season from August to October. August and September clearly stand out when it comes to variability in the dataset (as seen by the vertical extent of percentiles in Figure 3.3b), and the range in these months are greatest as well. The small variability in the winter season is partly due to the fact that huge areas are completely ice covered during winter season, limiting the opportunity of sea ice extent variability.

(a) *Seasonal cycle*

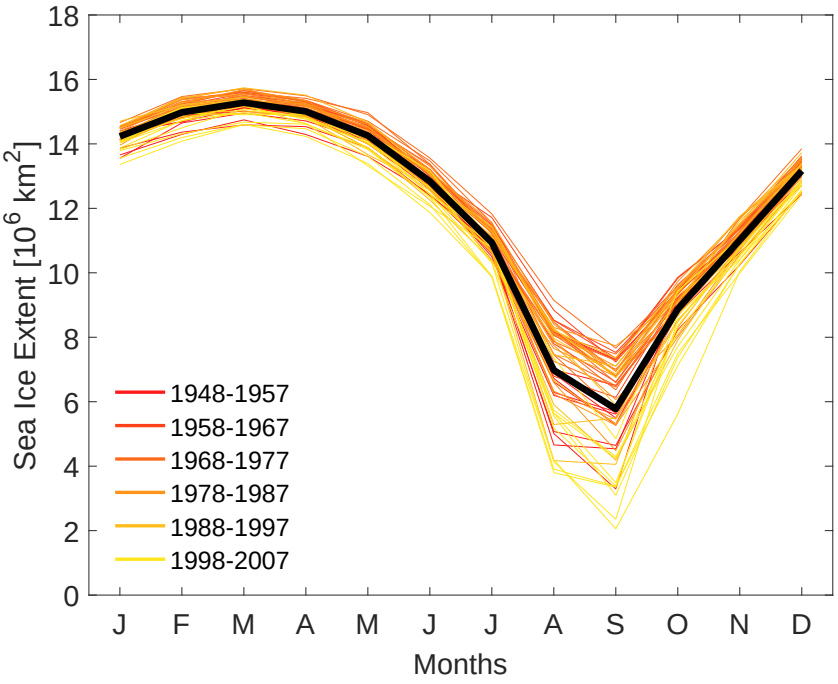

(b) *Boxplot of the seasonal cycle*

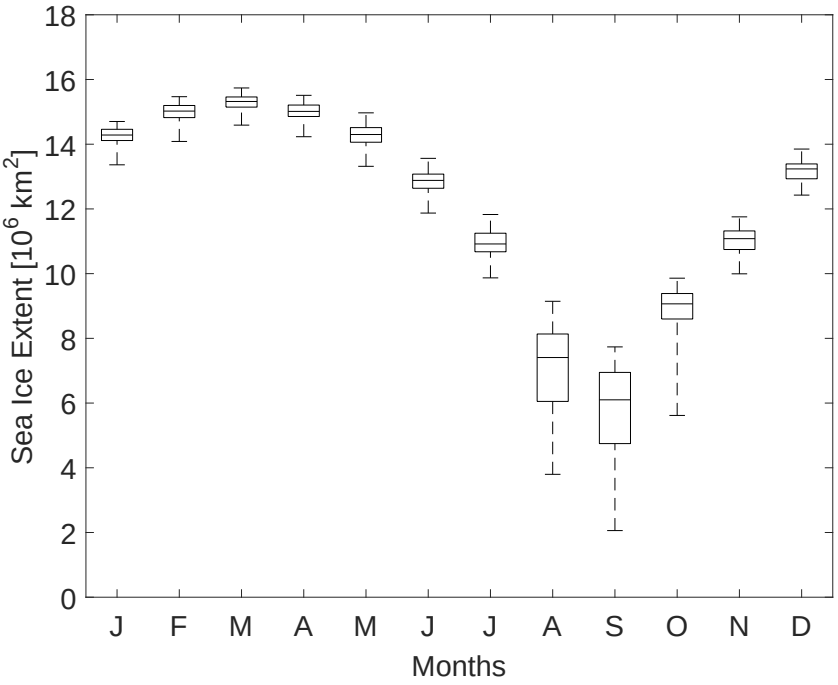

Figure 3.3: *All seasonal cycles (monthly mean) for the Northern Hemisphere sea ice extent from 1948 to 2007 (upper panel). The data is divided into 6 decades, where each color represents one decade, and yellow colors indicate later years. The lower panel shows the corresponding boxplot of the dataset, where the central mark represents the median, the edges of the box are the 25th and 75th percentiles, and the whiskers extend to the most extreme data points.*

3.3.2 Study regions

There are qualitative regional and seasonal differences in sea ice extent, e.g., as indicated in Figure 3.2 and Figure 3.4. The latter figure shows the seasonal cycles for each of the 12 Arctic regions that are defined in Figure 1.3, and for all 60 years in this study. The colored lines are individual years colored by decades from the beginning (red lines) to the end (yellow lines) for the period 1948 to 2007 (the colors representing each decade are shown in Figure 3.3). The thick black line indicates the mean seasonal cycle in that region over the whole study period. In this section, the mean line will be used as a basis for the description of the sea ice extent in each region, as it represents the average value of sea ice extent for each month of the year, hence attenuating the large interannual variations.

Most of the regions are similar to the seasonal cycle in the Northern Hemisphere (Figure 3.3a). However, some of the regions have a slightly flat maximum in the winter time, or a flat minimum in the summer time. A flat maximum that extends over several months indicates that the region is completely ice-covered during the winter season, and the region is not experiencing variations in the sea ice cover in these months. There are seven of 12 regions that experience a total cover of sea ice in the winter season, and they are a) Beaufort Sea which is completely ice-covered from November to May (on average), b) Chukchi Sea which is completely covered from December to May, c) East Siberian Sea covered from November to June, d) Laptev Sea covered from November to May, e) Kara Sea covered from December to May, i) Canadian Archipelago covered from November to June and j) Central Arctic that is completely ice-covered from October until July. Note that these values are averages, and that there are individual years that experiences earlier melting or later freezing. On the other hand, the flat minimum in the summer time over several months indicates that the region is completely ice-free during the summer season. This is a fact for the two regions k) Bering Sea and l) Sea of Okhotsk, which are ice-free during the summer months (July to October). The remaining three regions are neither totally ice-covered in winter nor ice-free in the summer, but they vary throughout the year. Therefore, these regions have seasonal cycles that are shaped like a sine wave, and their appearance is more similar to the seasonal cycle for the entire Northern Hemisphere (Figure 3.3a). These three regions are f) Barents Sea, g) Greenland Sea and h) Baffin Bay.

When it comes to the mean seasonal cycle (black line), all of the regions that are not completely ice-covered during winter have their maximum sea ice extent in March, except for f) Barents Sea that reaches its highest values in April (even though the average sea ice extent in March is very close). Furthermore, all of the regions that are not completely ice-

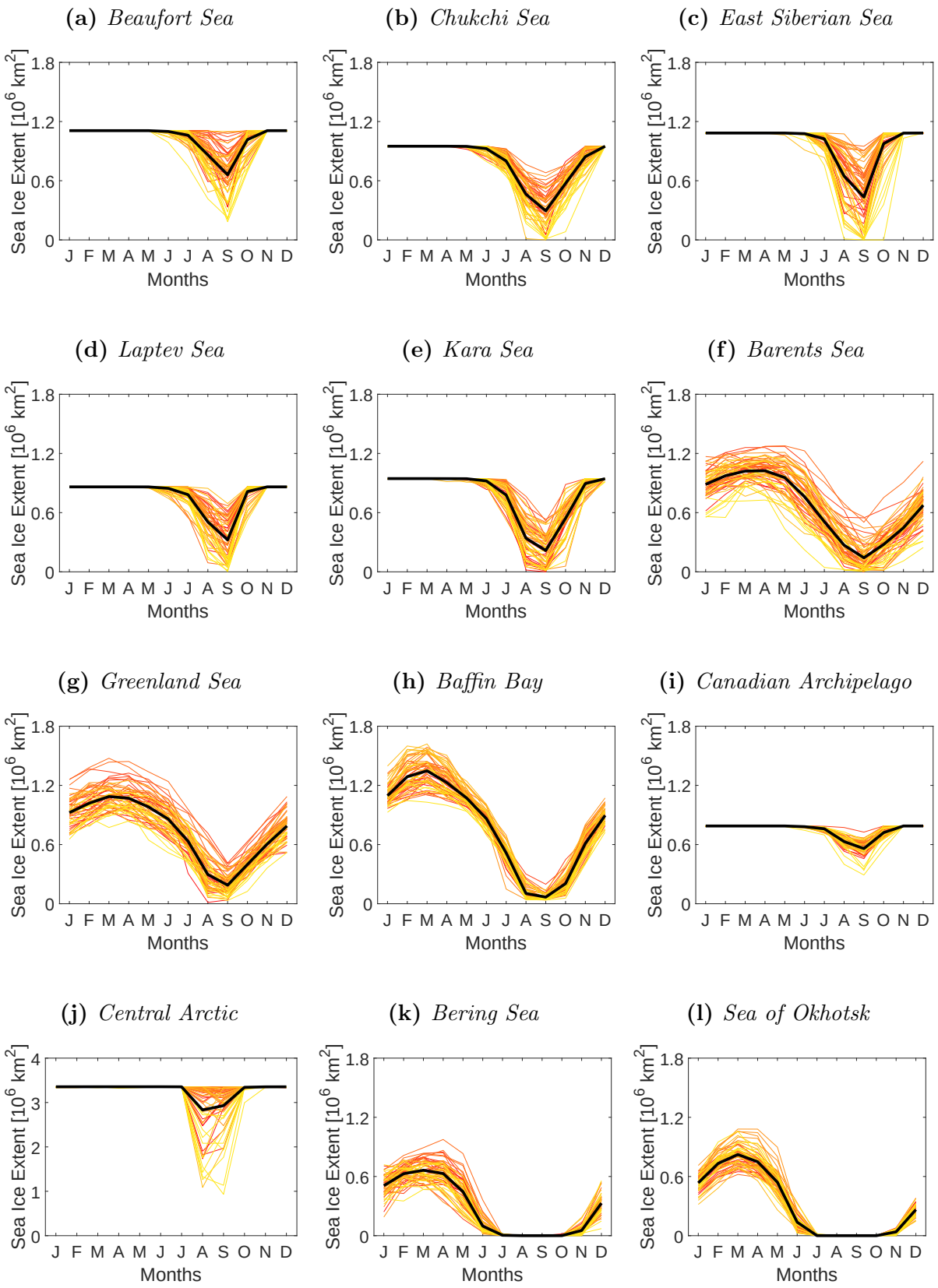

Figure 3.4: *Seasonal cycles for the different regions in the Arctic Ocean. The data is divided into 6 decades (1948-2007), where each color represents one decade (see 3.3a). The thick black line is the monthly mean value over the entire period. Note that the ranges are the same for all of the panels, except for j) Central Arctic.*

free during the summer months have their minimum sea ice extent in September, except for j) Central Arctic that reaches its lowest values in August.

The regions also have their greatest interannual variations in different months of the year. The regions with a total sea ice cover during winter typically have the largest interannual variations in September, when the sea ice extent in the region is lowest. The regions with open water during the summer season typically have the greatest interannual variations in spring (March and April). The three regions with the largest interannual variability throughout the year are neither totally ice-covered in winter nor totally ice-free during summer. This applies to f) Barents Sea, which has more or less variations on the same magnitude in all months of the year on average, while the other two regions g) Greenland Sea and h) Baffin Bay have greatest variations from February to April (in winter).

From the seasonal cycles for the different regions it is observed that some of the regions have been completely ice-covered the entire year in the simulated data. This can be seen by the fact that some of the lines are completely horizontal for all months in the seasonal cycle for individual years, and there are mostly red lines representing earlier years. Regions that have been completely ice-covered 12 months of the years in the study period are a) Beaufort Sea and j) Central Arctic, while regions experiencing a full ice cover 11 months of the year are c) East Siberian, d) Laptev Sea and i) Canadian Archipelago. Some of the regions also have been completely ice-free in at least one month in the 60-year study period, including b) Chukchi Sea, c) East Siberian Sea, d) Laptev Sea, e) Kara Sea, f) Barents Sea and g) Greenland Sea. Four of the latter regions are also completely ice-covered in winter, and have thus experienced a full ice-cover as well as completely ice-free conditions in the study period. This applies to all regions except for e) Kara Sea and f) Barents Sea.

3.4 Sea ice extent trends

In this section we will describe trends in sea ice extent for Period I (1948-1967) and Period III (1988-2007) in each of the 12 regions (Figure 1.3), and in the next section trends in sea ice concentration are described. This is due to the fact that they give slightly different values. The first period (Period I) includes the first two decades in the model simulation, which are characterized by increasing sea ice extent, while the second period (Period III) includes the last two decades in the model simulation, characterized by decreasing sea ice extent. During Period II (1968-1987) the sea ice extent is relatively stable (see Figure 1.2), so the trends in this period will therefore not be shown. Hereafter, the periods with increasing and decreasing sea ice cover will be referred to as Period I and

Period III, respectively. The trends in Table 3.2 are shown in percent change per decade, and are compared to the mean annual sea ice extent in each of the 12 Arctic regions calculated over the entire study period (the annual mean sea ice extent in each region is indicated in Figure 3.2). The trends in each month (March and September) and in each period (Period I and Period III) in Table 3.2 are comparable, because they are divided by the same number. However, the trends in the different regions are divided by different numbers, as the mean sea ice extent (over the entire study period) vary from region to region. All of the trends sea ice extent are generally greater in September than the trends seen in March, except for the Baffin Bay. Note that the trends are very sensitive to start values and end values in the relatively short time series.

Six of the regions in Table 3.2 show no trend in sea ice extent in March, and there are two regions in September showing no trend. These are the regions which are completely ice-covered in March, and the regions with no sea ice in September, respectively. However, there are seven regions that are completely covered with ice in March. The Central Arctic shows a trend, despite the fact that it is on average completely ice-covered in March. This region is in fact not completely ice-covered in March in every year in the study period, and changes in individual years are so small that they are hidden behind the average March value (black line in Figure 3.4j). Note that these trends are not statistically significant and that these trends are very small (0.03 % change per decade in Period I and - 0.02 % change per decade in Period III).

The greatest trends in March during Period I are seen in the Barents Sea, the Greenland Sea and the Sea of Okhotsk. These are also the only trends in March in Period I that are significant on the 5 % level (marked bold in Table 3.2), calculated by the p-value (described in Section 2.3.4). The only region with negative trends with respect to the 1948 to 2007 regionally mean sea ice extent, is Baffin Bay, but note that this trend is not significant. In Period III for March, the dominant trend occur in the Baffin Bay, with the largest negative trend of - 30.45 % change per decade. This trend is also the only significant trend on the 5 % level in this period in March in Table 3.2. The Bering Sea also shows a large negative trend in March, followed by the two regions with large positive trends in Period I, namely the Greenland Sea and the Barents Sea.

Almost all trends in September are significant, both for Period I and for Period III, except for the trends in the Canadian Archipelago, which also clearly shows the weakest trend, and Laptev Sea in Period I. All trends in Period I in September are positive, and the strongest trends are seen in the East Siberian Sea, the Beaufort Sea, the Barents Sea and the Chukchi Sea, respectively. In Period III for September, the largest trends occur in the

Table 3.2: *Regional linear least-square trends of the sea ice extent, shown in percent change per decade [%/decade], calculated from the annual mean sea ice extent for each region over the period 1948-2007 (see Figure 3.2 for approximate values of the mean annual sea ice extent in each region). Trends are calculated for each Arctic region for Period I (1948-1967) and Period III (1988-2007) for the months with sea ice extent maximum (March) and minimum (September). The bold numbers are statistically significant at the 5 % level.*

		Beau.	Chuk.	East	Lapt.	Kara	Bare.	Gree.	Baff.	Cana.	Cent.	Beri.	Okho.
March [%/decade]	**I**	0	0	0	0	0	**19.53**	**19.31**	-2.80	0	0.03	8.37	**17.96**
March [%/decade]	**III**	0	0	0	0	0	-6.61	-7.71	**-30.45**	0	-0.02	-16.44	4.39
September [%/decade]	**I**	**19.98**	**17.24**	**22.06**	12.35	**16.21**	**18.14**	**13.17**	**4.26**	5.78	**10.57**	0	0
September [%/decade]	**III**	**-24.28**	**-20.72**	**-22.31**	**-23.56**	**-22.99**	**-15.65**	**-10.35**	**-2.77**	-7.95	**-22.93**	0	0

Beau. is Beaufort Sea, Chuk. is Chukchi Sea, East is East Siberian Sea, Lapt. is Laptev Sea, Kara is Kara Sea, Bare. is Barents Sea, Gree. is Greenland Sea, Baff. is Baffin Bay, Cana. is Canadian Archipelago, Cent. is Central Arctic, Beri. is Bering Sea and Okho. is Sea of Okhotsk

Beaufort Sea, the Laptev Sea, the Kara Sea, the Central Arctic, the East Siberian Sea, and the Chukchi Sea, respectively. Even though the trends for the Central Arctic are not greater relative to the other trends, note that this area contains over three times more sea ice than all the other areas. A change on the same magnitude as the other areas thus represents a larger sea ice loss in million km^2, meaning that the total loss of sea ice in September is thus dominated by the sea ice loss in the Central Arctic.

3.5 Sea ice concentration trends

Figure 3.5 shows the spatial distribution of the linear trends in sea ice concentration in March and September for the two periods Period I (from 1948 to 1967), and Period III (from 1988 to 2007), as defined in Figure 1.2. Red values in Figure 3.5 indicate that the sea ice concentration has a positive trend, while blue values represent a negative trend in sea ice concentration. Table 3.2 shows the trends for the sea ice extent for the same two periods as the trends in sea ice concentratons in Figure 3.5, and for the same months (March and September). The trends in sea ice extent and the trends in sea ice concentration show slightly different values, and the reason for these differences will be discussed in Section 4.3.

There are large differences between the two periods, as well as between the winter and summer seasons. From Figure 3.5, it is clear that the sea ice cover is located at different places in March and September. This can be seen from, e.g., the areas with no change at all, and the outermost trends which show the continuously shifting ice edge. These changes occur naturally due to the fact that the location of the ice edge is very dynamic and has large seasonal and interannual variations. These variations are influenced by, e.g., interannual temperature changes in the ocean and the atmosphere, local weather, ocean currents and wind conditions. The sea ice concentration in Period I shows both positive and negative regional trends in March, and only positive trends in September. The sea ice concentration in Period III shows only negative trends, both in March and September.

Strong positive trends in March in Period I occur in the Barents Sea, Greenland Sea and Sea of Okhotsk, as was also seen for the trends in sea ice extent in Table 3.2. The strongest negative trends in Period I occur in a few areas in Baffin Bay and Bering Sea, and weaker trends are seen typically near land areas in the eastern Arctic Ocean and to the north of Greenland (in the Eurasian basin). In Period III, however, there are no strong positive trends for the March sea ice (neither in Figure 3.5 nor Table 3.2). The

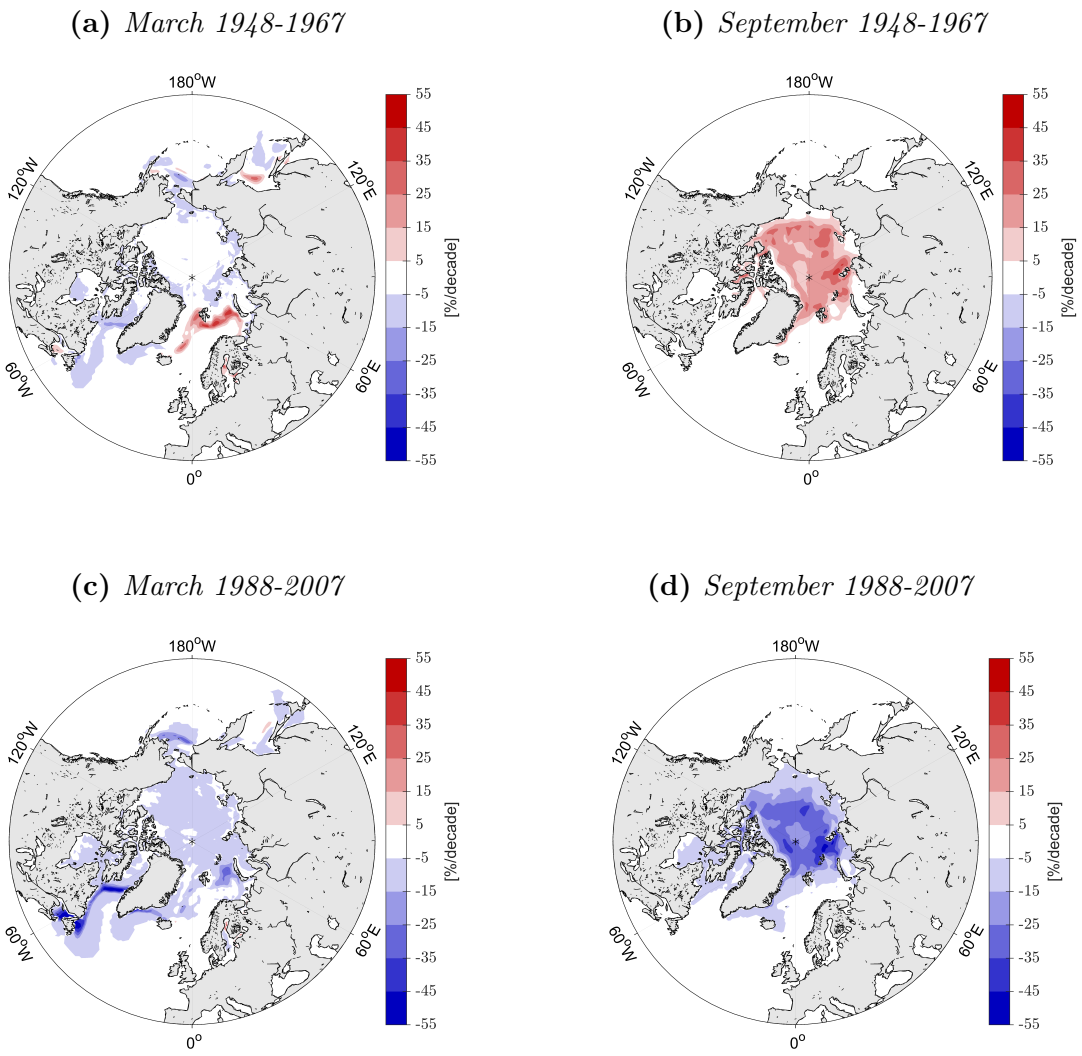

Figure 3.5: *Sea ice concentration trends for March and September for Period I (1948-1967) and Period III (1988-2007), calculated by the linear least-squares method (see Section 2.3.6).*

strongest negative trends in March in Period III are seen in the Baffin Bay (as is also seen in Period I, and for the sea ice extent with - 30.45 % change per decade), the Barents Sea (which has a relatively strong positive trend in Period I), and the Bering Sea. These regions also show relatively strong negative trends in sea ice extent in Table 3.2 in this period. Negative trends in sea ice concentration are generally seen in the Arctic Ocean in Period III as well, however the trends are not confined to the land areas in Period III, as is seen in Period I. The negative trends in Period III are thus present in the entire Arctic Ocean, also in central parts.

For the September values, the strongest positive trends are seen in Period I in Laptev Sea

and East Siberian Sea (which also has a strong trend in sea ice extent in this period), but also generally in central parts of the Arctic Ocean. There are no negative trends in Period I for September sea ice concentration. In contrast, there are no positive trends in September in Period III. In this period, the negative trends are present in the entire Arctic Ocean, and the trends are strongest in the Kara Sea and in central parts of the Arctic Ocean. The negative trends can also be seen south of the Arctic Ocean on the Atlantic side close to Greenland, as well as near Canada to the west of Greenland in Baffin Bay.

The trends in sea ice extent in Table 3.2 show similar results as the trends in sea ice concentration in Figure 3.5. However, there are differences between the trends in these two measures of the sea ice cover (e.g., in the Barents Sea). It is thus interesting to compare the trends in sea ice extent described in the previous section and the trends in sea ice concentration in this section in March and September, and for the two time periods. This will be discussed in Section 4.3.

3.6 Sea ice concentration anomalies

Figure 3.6 shows the anomalies in sea ice concentration in 2007 for March and September, relative to the 1948 to 2007 mean, for the two months with maximum and minimum sea ice extent, respectively. A figure showing the spatial distribution of the sea ice concentration in March and September 2007 are shown in Figure 3.1e) and Figure 3.1f), respectively. The year 2007 is chosen because it is the year with the smallest annual mean sea ice extent in the simulation in the entire study period in the Northern Hemisphere (see Figure 1.2). However, from later observations we know that the sea ice extent reached even lower values in 2012.

The majority of the anomalies in Figure 3.6 are negative, both in March and in September, representing areas with lower sea ice concentration than the average for the reference period from 1948 to 2007.

In March (Figure 3.6a), the strongest negative anomalies occur in the Barents Sea and in the Greenland Sea. There are also relatively strong negative anomalies in parts of the Baffin Bay, Bering Sea and Sea of Okhotsk. Only a few positive anomalies can be seen in the sea ice concentration, with the greatest positive anomalies in the Pacific Ocean in the Bering Sea and Sea of Okhotsk. An interesting finding, is that the anomalies in the sea ice concentration are mainly found in the eastern Arctic Ocean (0-180°E) in March 2007, while there is almost no anomalies in the western region (0-180°W). Note that the entire Arctic Ocean is covered by sea ice in March 2007 (see Figure 3.1e), so

the negative anomalies mean that the grid cells contain a lower percentage of ice than average. However, there is no change in sea ice extent because the grid cells exceed 15 % sea ice concentration .

In September 2007 (Figure 3.6b), there are mainly negative anomalies, except from two small areas in the Beaufort Sea and in the Canadian Archipelago, as well as a tiny area east of Svalbard. The strongest negative anomalies are located in the central Arctic Ocean, and decreases slightly southward towards land areas. However, the negative anomalies cover the entire Arctic Ocean, as well as in the western part of the Atlantic Ocean and west of Greenland in the Canadian Archipelago.

As mentioned previously in this section, the anomalies show that the sea ice concentration in a few areas in the Sea of Okhotsk and in the Bering Sea is particularly high in March 2007, compared to the mean sea ice concentration. This can be seen in Figure 3.1e) as well, as the sea ice cover in 2007 in these areas in fact are comparable to the sea ice cover in 1979, which is a year with a lot more sea ice than 2007.

Furthermore, the anomalies of sea ice concentration in 2007 (Figure 3.6) are compared to the linear trends in sea ice concentration (Figure 3.5) in the last period, Period III (1988-2007). The trends are described in Section 3.5, and it is interesting to see that the anomalies seen in this specific year more or less correspond to the long-term trends in the last two decades in the model simulation. In March, the long-term trends are strongest in Baffin Bay, Barents Sea and Bering Sea, which are also the regions with the strongest anomalies in 2007 for March. However, the area in the Bering Sea (close to Alaska) has a positive anomaly where the long-term trend is negative. In this period, the 20-year trend also shows negative values in the entire Arctic Ocean, where the anomalies in 2007 are more confined to the eastern part of the Arctic Ocean. For the September sea ice concentration, the trends are negative in the entire Arctic Ocean, with the strongest trends in the central parts of the ocean, and near the Kara Sea. The anomalies show the same result (negative anomalies), except that they are not greater in the Kara Sea compared to other regions.

(a) *March 2007*

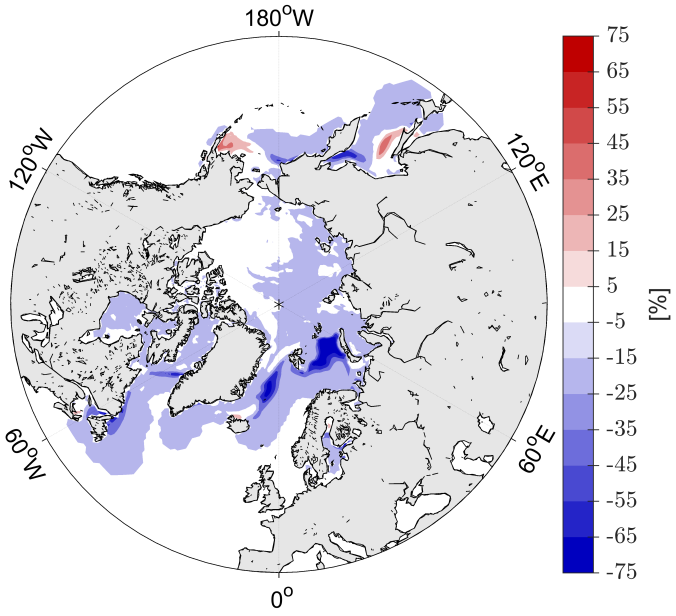

(b) *September 2007*

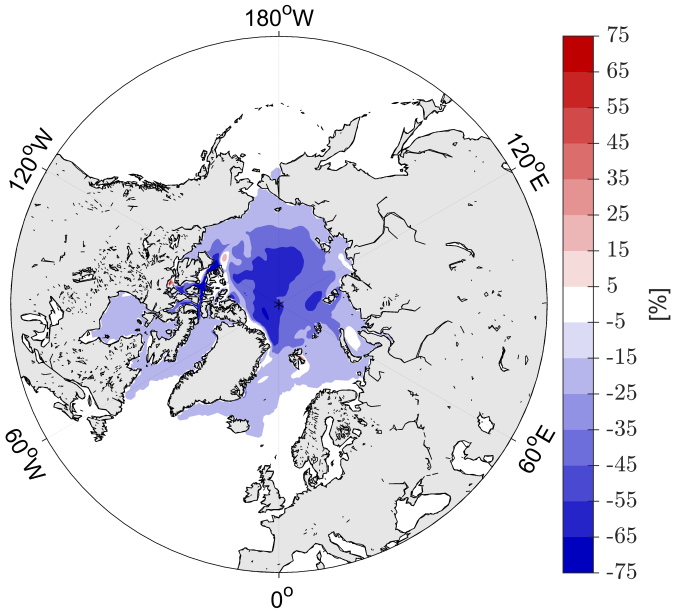

Figure 3.6: *Sea ice concentration anomalies in the Arctic Ocean for the year 2007. March anomalies are calculated from the mean sea ice concentration in March (1948-2007), and September anomalies are calculated from the mean sea ice concentration in September (1948-2007).*

Chapter 4

Discussion

In this chapter the central results achieved in the previous chapter are discussed and compared to existing literature related to these findings, and the model simulation is also compared to observations. These observations are for the entire Northern Hemisphere (shown in Figure 1.2), however this chapter will also focus particularly on the Barents Sea. Further, it will be discussed whether the sea ice in the Arctic experiences increased melting towards summer, or if decreased freezing towards winter is the dominant cause in the diminishing Arctic sea ice cover.

4.1 Comparison of the model simulation and in-situ observations

This section will mainly discuss and compare the model simulation to observations in the period before the satellite era, meaning that the measurements are retrieved from in-situ observations. Both in-situ observations from the ocean and from the atmosphere are used in this comparison. A strength of model simulations is that they provide data from a long time before satellite observations are available. In this thesis the model simulates 32 years before the satellite observations started, which means that the dataset from the model simulation contains 60 years in contrast to the 37 years of available observational data from satellites. However, in-situ observations, e.g., of air temperatures and sea surface temperatures, are available for several locations before the satellite era. By comparing in-situ data to the model simulation in the period they have in common (1979-2007), they can give us more information about the changes and variability in the atmosphere and in the ocean, and hence probably of the sea ice as well. This will be brought up because it provides an insight into how realistic the model simulation is, compared to what is observed. However, note that the model is forced with atmospheric reanalysis data.

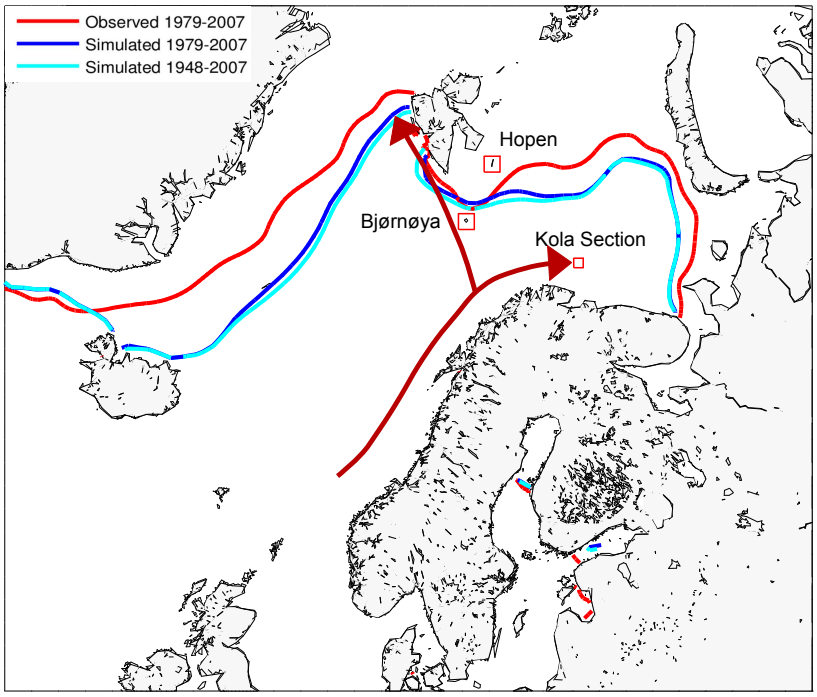

Figure 4.1: *The location of the sea ice edge (15 % ice concentration) found from observations averaged over the period from 1979 to 2007 (red), from the model simulation averaged over the same period from 1979 to 2007 (dark blue), and the model simulation averaged over the entire study period from 1948 to 2007 (light blue). In addition, the location of Bjørnøya, Hopen, and the Kola Section (red squares) are shown. The dark red arrows show Atlantic water entering the Barents Sea, as well as the West Spitsbergen Current going northward west of Svalbard.*

The Barents Sea has some of the greatest interannual sea ice variability of all regions in this study (Figure 3.2f), and additionally some of the strongest trends in sea ice concentration in winter occur in this region (Figure 3.5a and Figure 3.5c). This region also accounts for much of the variance of sea ice in the entire Northern Hemisphere in Period III (1988-2007), as seen in Table 3.1. Additionally, the largest sea ice retreat is predicted to occur in the Barents Sea in the future (Koenigk et al., 2013). Therefore, this section will mainly focus on one specific location - the Barents Sea. There are available in-situ observations for the ocean temperature in the Kola Section (0-200m depth) and for air temperatures from Svalbard, Bjørnøya and Hopen, which are located in the Barents Sea (their locations are shown in Figure 4.1). This figure also shows that the model simulation has a larger sea ice cover than what is observed in the Barents Sea. This is in contrast to what is seen for the entire Northern Hemisphere, where the simulated sea ice extent is underestimated

(Figure 1.2). This interesting finding will be discussed in Section 4.4. The sea ice edge for the model data in the period from 1979 to 2007 is located slightly north of the sea ice edge for the model data in the entire study period from 1948 to 2007. This is expected because the sea ice extent is greater in the period before 1979 than after (Figure 1.2).

4.1.1 Air temperatures and sea ice extent in the Barents Sea

Figure 1.2 shows that there is a period with increasing sea ice extent in the Northern Hemisphere until the end of the 1960s (Period I), a period with stable sea ice extent until the 1980s (Period II), followed by a period of decreasing sea ice extent to the end of the study period (Period III). This may suggest that the temperatures in the atmosphere and in the ocean have changed significantly over these periods, as temperature strongly affects and influences the melting and freezing of sea ice. Although satellite observations are not available before the year of 1979, observations of air temperatures from a permanent weather station on Svalbard have been available since 1911. Since 1950 observational temperatures have been available from stations situated on Hopen and Bjørnøya as well, which are two islands located in the Barents Sea (their locations are shown in Figure 4.1).

Figure 4.2 shows the air temperature observations from Førland et al. (2012) from weather stations at Hopen, Bjørnøya and Svalbard. The figure shows that the temperatures vary simultaneously, and that there are large decadal variations in the data. These features are also seen for other parts of the Arctic, according to Førland et al. (2012). Førland et al. (2012) analyzed two decades at a time, and relevant to this study are the periods from 1943 to 1965, 1966 to 1988 and 1989 to 2011. The observations show that there was a cooling period from 1943 to 1965 that was particularly strong, and the stations on Svalbard showed temperature trends of -1.5°C to -1.8°C per decade, while the next two decades from 1966 to 1988 were more stable with trends of 0.5°C to 0.7°C per decade, and the last two decades from 1989 to 2011 had even stronger temperature trends with 2°C to 3°C per decade in winter at all stations. All in all, the temperatures decreased from the 1950s to the end of the 1960s at all stations, followed by a temperature increase at all stations (with a few smaller variations) that extends until 2011. This is consistent with the periods of variations seen in the sea ice extent in Figure 1.2 and the trends in sea ice in Table 3.2 and Figure 3.5. As Figure 3.2f), 3.2g) and 3.2j) show, the sea ice extent in the surrounding seas of Svalbard, Hopen and Bjørnøya - the Barents Sea, the Greenland Sea and the Central Arctic - had an increase in sea ice extent until the end of the 1960s, concurrent with this cooling period, followed by a period of decreasing sea ice extent.

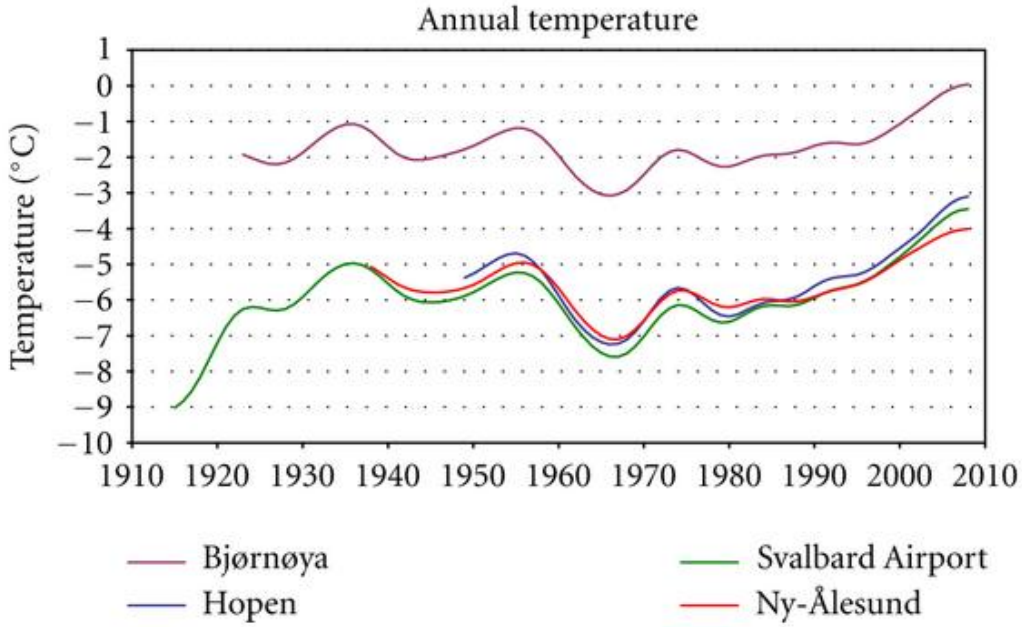

Figure 4.2: *Air temperature observations from Bjørnøya, Hopen and two different stations located on Svalbard from 1911 to 2011 (figure from Førland et al., 2012). The time series have been low-pass filtered, and show variability on a decadal time scale. In addition, the first and last three years of each of the curves have been cut out.*

This suggests that the sea ice in the model simulation corresponds well with the in-situ observations of increasing air temperatures, which it also should, as the model simulation is forced with atmospheric reanalysis data at the surface. Note that air temperatures in the Svalbard region in general are highly sensitive to both the sea surface temperature as well as the ice cover (Førland et al., 2012).

The recent global temperature rise, with amplified Arctic temperatures, is closely linked to the reduction of the Arctic sea ice cover (Dobricic et al., 2016). It is suggested that regions with large sea ice loss, like the Barents Sea, can impact the atmosphere in the entire Northern Hemisphere (Petoukhov and Semenov, 2010). In fact, the recent winter reduction of sea ice in the Barents Sea area is largely contributing to the total winter sea ice reduction seen in the entire Arctic (Figure 3.5c). Actually, near-surface heating in the Barents Sea and the Kara Sea caused by the reduction of sea ice can lead to anticyclonic anomalies over the Arctic Ocean. This causes easterly advection over northern continents, and results in a winter cooling with increased probability of cold winter extremes over Europe (Petoukhov and Semenov, 2010). This is in agreement with expected consequences of global warming.

4.1.2 Ocean temperatures and the sea ice extent in the Barents Sea

In-situ observations of ocean temperature (0-200m depth) are available from the Kola Section a few decades before sea ice observations from satellites started (Figure 4.3). The data in Figure 4.3 is provided by PINRO - Knipovich Research Institute of Marine Fisheries and Oceanography, Russia through the International Council for the Exploration of the Sea (ICES)[1]. The Kola Section is located in the Barents Sea, along the main pathway of the Atlantic water entering the Arctic Ocean (Figure 4.1 shows the location of the Kola Section, as well as the pathway for the Atlantic water). The relatively warm Atlantic water meets the cold Arctic atmosphere, resulting in a large heat flux from the ocean to the atmosphere in winter. This heat flux is essential for the formation of sea ice, as sea ice does not form before the ocean reaches the freezing point. As soon as sea ice has formed, the heat flux instantly reduces, since the sea ice works as a lid on the ocean, hence limiting the heat transfer between the ocean and the atmosphere. In fact, the Atlantic heat transport has been anomalously high recently, and has resulted in a decrease in the sea ice extent in the Barents Sea during the winter season (e.g., Smedsrud et al., 2013; Årthun et al., 2012).

The Atlantic currents bring relatively warm Atlantic water into the Barents Sea and the Greenland Sea from lower latitudes (Figure 4.1), and explains the receding sea ice edge in areas adjacent to the Norwegian Atlantic Current and the West Spitsbergen Current (Kvingedal, 2005; Onarheim et al., 2014). As seen in Figure 4.3, the observed ocean temperature in the Kola Section has increased in recent years, suggesting that this increased Atlantic heat transport reaches the Kola Section. The observed ocean temperature in the Kola Section and the simulated sea surface temperature in the Kola Section (both detrended) have a correlation of $r = 0.70$ in the period from 1951 to 2007, meaning that 49 % of the variance is statistically explained (significant on the 5 % level). The rather high correlation, $r = 0.70$, means that the observed ocean temperature in the Kola section and the simulated sea surface temperature are comparable. However, although the interannual variability is highly correlated, the mean state differs. The observed ocean temperature (0-200m depth) is about 1°C warmer than the simulated sea surface temperature (Figure 4.3a). In fact, Bentsen et al. (2012) showed that the sea surface temperature in NorESM is between 0.5°C and 2.5°C colder than the observed sea surface temperature from 1979 to 2005 in the Barents Sea. Even though this applies to the sea surface temperature, it is likely to apply to the deeper layers as well. The fact that the model simulation has lower ocean temperatures in this region may also contribute to

[1] http://ocean.ices.dk/iroc/

(a) *Observed ocean temperature and simulated sea surface temperature*

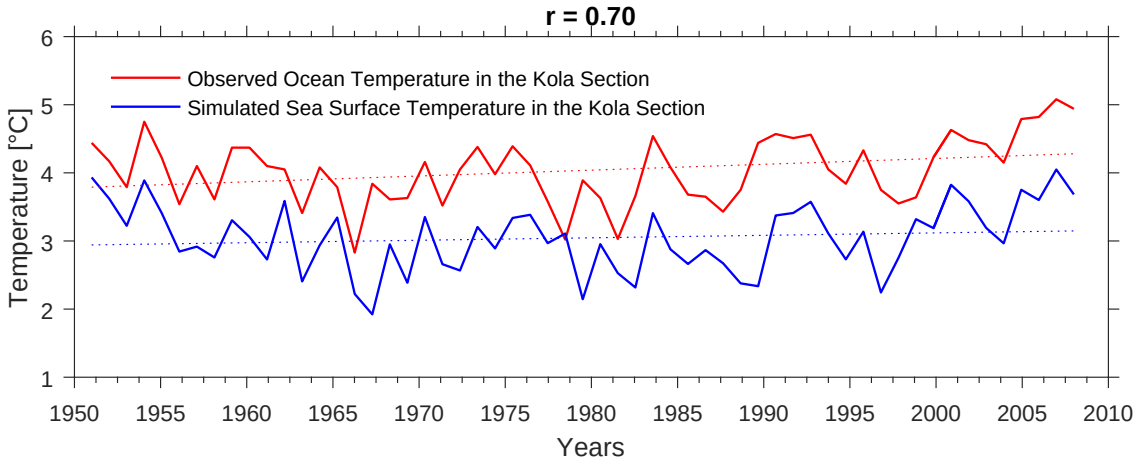

(b) *Simulated sea surface temperature and simulated sea ice extent*

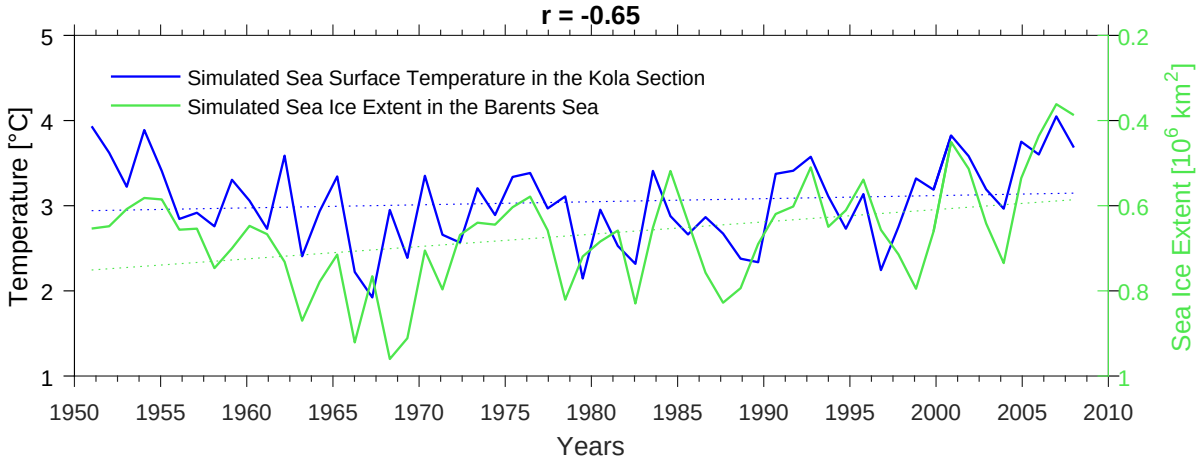

Figure 4.3: *a) shows observations of annual mean ocean temperature in the Kola Section (0-200m depth) and the simulated annual mean sea surface temperature in the Kola Section, during the period from 1951 to 2007. Simulated annual mean sea surface temperature and the simulated sea ice extent in the entire Barents Sea is shown in b). Note that the sea ice extent is reversed to make it easier to compare the two time series, and that the vertical axis for the sea ice extent is shown on the right side of the graph. The dotted lines show the linear trends for each dataset, and the correlation coefficient, r, between the detrended time series are shown at the top of each panel.*

the fact that the sea ice edge in the Barents sea and adjacent seas are farther to the south than what is observed (Figure 4.1), as lower ocean temperatures provide better conditions for sea ice formation, hence the sea ice cover expands.

Further, the simulated sea surface temperature in the Kola Section and the simulated sea

ice extent in the Barents Sea are shown in the lower panel of Figure 4.3. These time series have a correlation coefficient of $r = -0.65$, meaning that they are anti-correlated and vary in the opposite direction (when, e.g., the temperature increases, the sea ice extent decreases). This indicates that the simulated sea ice cover and ocean temperatures in the Barents Sea are tightly coupled in NorESM, as is expected from observations.

4.2 Comparison of the model simulation and satellite observations

As shown in Figure 1.2, the simulated Northern Hemisphere sea ice extent is less than what is observed at all times in the annual mean time series, and Wang et al. (2016) shows the same result. On the other hand, the seasonal cycle of the sea ice extent illustrated in Figure 1.2 shows that the observed extent is not consistently greater for each month of the year. In fact, the model and the observations show almost the exact same values for the sea ice extent from October to December, during the freeze-up period of the sea ice cover. This period is associated with relatively low incoming solar radiation in the Arctic region, meaning that the atmosphere is colder than the ocean, since the ocean holds heat more effectively. When the ocean finally has cooled down to the freezing-point, formation of sea ice begins. As mentioned in the previous section, this sea ice works as a lid on top of the ocean, limiting the heat exchange through the ocean-atmosphere interface. In addition, the model is driven by forcing from atmospheric reanalysis that is based on observations, hence the atmospheric reanalysis knows where the ice edge is. Because of this, the reanalysis has a large flux from the ocean to the atmosphere over open ocean, and a small flux from the ocean to the atmosphere when sea ice is present in the reanalysis. NorESM will thus lose a large amount of heat in places with open water and will therefore form sea ice at that location, whilst at other places the heat loss is less in NorESM, and the ocean will remain open. This corresponds well with the observed sea ice cover, because the atmospheric fluxes are adapted to the ice edge. As a result, the sea ice extent in the model simulation can be very similar to the actual observations in the freeze-up period.

However, the model overestimates the sea ice extent in the melting period from April to July. In this period, it is harder for the model to know where the ice will be melting and how fast it melts. There are many factors that contribute to the melting of sea ice, including solar radiation, temperatures in the atmosphere as well as the ocean and the thickness of the sea ice. NorESM is known to generally overestimate the sea ice thickness compared to the observations (Bentsen et al., 2012), and this factor can contribute to the overestimation of sea ice extent (April to July) in the melting period of the sea ice

cover (see the inset in Figure 1.2), as it takes more time for thicker ice to melt completely. However, NorESM underestimates the sea ice thickness in March (Wang et al., 2016). It is unclear whether this underestimation also extends to the upcoming melting period, but since the simulated sea ice extent has a less rapid decrease in the melting period than what is observed, and the model in addition lags the observations in this period, it may be a result of the overestimated sea ice thickness that is seen in general (Bentsen et al., 2012). The thicker ice may be a result from too slow summer melt, combined with weaker winds across the polar basin in NorESM than observed. Since the simulated sea ice is too thick, more heat is needed in order to melt the sea ice and produce open ocean in the melting season, if the forcing in the model simulation is similar to the forcing in the nature.

When the sea ice extent reaches its extreme values in March and September, the model underestimation of sea ice extent from the observations is by far the greatest. The underestimation of sea ice in March in the Northern Hemisphere can be a result of too little ice in the Labrador Sea (here defined under the Baffin Bay) in the NorESM model, which may be due to the warm SST bias in this area (Bentsen et al., 2012). In September, the sea ice cover in the model is probably thicker than the observations (as this is the general case for NorESM), in contrast to the thinner sea ice seen in NorESM in March (Wang et al., 2016). However, since the sea ice probably is thicker in summer and in addition has a larger extent in the model than in the observations, it is unclear why the simulated sea ice extent suddenly is underestimated in September. From July to August there is a sudden drop in sea ice extent, and huge amounts of ice suddenly melts. One can speculate why this is, but one possible explanation can be that there is one (or several) feedback mechanisms in the model that responds stronger in the melting process of sea ice in summer, making the sea ice melt faster towards September.

The correlation between the model simulation and the observations of the detrended time series in the period from 1979 to 2007 is calculated to be $r = 0.73$ (Figure 1.2), meaning that the model simulation captures 53 % of the observed sea ice variability. This rather high correlation means that the sea ice extent in the model and the sea ice extent in the observations are closely linked together concerning interannual variability, even though the model underestimates the observed sea ice extent on a yearly average.

Other factors possibly causing differences between the model simulation and the observations, is the grid resolution in the model, parametrizations, choices of parameters and different snow and sea-ice albedo treatments in the sea ice model used (Danabasoglu et al., 2014). Note that the Arctic region and processes in high latitudes, including the seasonal

cycle of the sea ice cover, are very challenging to simulate accurately, due to the choice of atmospheric boundary conditions and model configurations (Griffies et al., 2009).

The last year in the model simulation, 2007, is also the year with the smallest annual mean sea ice extent in the entire study period in the model simulation in the Northern Hemisphere (see Figure 1.2). From later observations, we know that the observed sea ice extent in 2012 was even smaller than the sea ice extent in 2007. The declining sea ice extent in the Northern Hemisphere towards the end of the model simulation is clearly visible in the regional time series as well, e.g., in the sea ice extent in the Barents Sea (Figure 3.2f), the East Siberian Sea (Figure 3.2c) and for the Central Arctic (Figure 3.2j).

Recently, it is suggested that the recent loss of sea ice in the Arctic is responsible for the anomalously high temperatures in the Arctic (the Arctic amplification) in later years through sea ice-ocean feedbacks (Overland and Wang, 2010).

4.3 Comparison of trends in sea ice extent and sea ice concentration

Trends in sea ice extent and trends in sea ice concentration are described in Section 3.4 and Section 3.5, respectively. As shown in Table 3.2 and Figure 3.5, the trends in sea ice extent and sea ice concentration are slightly different for different Arctic regions. Sea ice concentration (as explained in more detail in Section 2.2.1) refers to the concentration of sea ice in each grid cell, while the sea ice extent is the extent made up of grid cells with concentrations higher than 15 % of sea ice (explained in more detail in Section 2.2.2). The differences between the trends in sea ice extent and sea ice concentration are especially clear in regions which are completely ice-covered in the winter season. A change from, e.g., 90 % sea ice concentration to 60 % sea ice concentration will not affect the sea ice extent, since the sea ice concentration is more than 15 %, and the grid cell is still defined as 100 % sea ice covered. The sea ice concentration, on the other hand, takes a change like this into account, and shows a negative trend of 30 % in this area.

Overall both sea ice extent and sea ice concentration indicate positive trends in Period I and negative trends in Period III, however with some seasonal and regional variations.

The regions which have a full sea ice cover in the winter season have no trend in sea ice extent during this period, since the sea ice concentration exceeds 15 %. However, since there is a change in sea ice concentration, Figure 3.5 clearly shows non-zero trends in

March. This applies to the Beaufort Sea, the Chukchi Sea, the East Siberian, the Laptev Sea, the Kara Sea, but also the Central Arctic shows very small trends. These regions show no trends at all in the sea ice extent in March neither in Period I nor in Period III in Table 3.2. However, Figure 3.5 shows small negative trends in the Chukchi Sea, the Laptev Sea and the Kara Sea in Period I, and in Period III there are negative trends in all of these regions (between 0 and 10 % change per decade in sea ice concentration over the two decades). For the ice-free regions in the summer season the trends are trivial both in Table 3.2 and Figure 3.5, which is the case for the Bering Sea and the Sea of Okhotsk. Hence, there is no difference between the trends in sea ice concentration and sea ice extent in this instance.

The strongest trends for Period I in September in Table 3.2 as mentioned in Section 3.4, are seen in the East Siberian Sea, the Beaufort Sea, the Barents Sea and the Chukchi Sea, respectively. From Figure 3.5b in Section 3.5, it also seems that parts of the East Siberian experiences the largest sea ice concentration trends in this period, however strong positive trends are seen in a few areas in the Laptev Sea as well. In Period III for September in Table 3.2, the largest trends occur in the Beaufort Sea, the Laptev Sea, the Kara Sea, the Central Arctic, the East Siberian Sea and the Chukchi Sea, respectively. Figure 3.5d, on the other hand, shows that the largest negative trend in sea ice concentration occur in the areas around the Kara Sea and in the Central Arctic.

It appears that the trends in sea ice concentration in the Barents Sea are stronger in March than in September, both in Period I and in Period III (Figure 3.5). On the other hand, Table 3.2 shows that the trends are similar in March and September in Period I, while the strongest trends in Period III are seen in September. As the greatest decline in sea ice extent in the Barents Sea happens during summer, the decreasing sea ice extent in the Barents Sea is thus associated with increased summer melting. However, this is in contrast to the trends in sea ice concentration, and to existing literature. Smedsrud et al. (2013) showed that the sea ice loss in the Barents Sea during winter is not caused by ice which has melted, but by ice that never formed. Additionally, Sandø et al. (2014) showed that an increased heat transport northwards results in less formation of sea ice in regions that are seasonally ice-covered during winter (like the Barents Sea), which in turn leaves less ice for melting during the next summer.
The trend in sea ice extent for the entire Northern Hemisphere is also calculated (not shown). For the period 1979-2006 the total change in sea ice in the model simulation is calculated to be $-42.35 \cdot 10^3$ km^2 per year. Parkinson and Cavalieri (2008) showed a negative trend of $-45.10 \cdot 10^3$ km^2 per year for the same period, meaning that the trend in the model data corresponds well with observations for the Northern Hemisphere in total.

4.4 Comparison of observed and simulated sea ice extent in the Barents Sea

An interesting finding in Section 4.1 showed that the sea ice edge in NorESM is located farther south (larger sea ice extent) than the observed sea ice edge in the Barents Sea (Figure 4.1). This is in contrast to the fact that the NorESM in general simulates less ice than what is observed in the Northern Hemisphere (Figure 1.2). Hence, this section will present and discuss the differences between the sea ice extent in the model and the observed sea ice extent in the Barents Sea.

Figure 4.4 shows the simulated and the observed sea ice extent in the Barents Sea, both for March (upper panel) and for September (lower panel). In agreement with the sea ice edges shown in Figure 4.1, there is a noticeable difference between the sea ice extent in the model and in the observations in the Barents Sea, which applies to both the winter season (March) and the summer season (September). Ilicak et al. (2016) show that there are cold biases in the NorESM model in the Atlantic, and water that is colder than observed is exported through the Davis Strait (in the Baffin Bay), the Barents Sea Opening and through Fram Strait. It has also been shown that NorESM generally simulates lower sea surface temperatures in the Barents Sea than what is observed (Bentsen et al., 2012), as mentioned in Section 4.1.2. This underestimation of the sea surface temperature in the Barents Sea is shown in Figure 4.3, where the observed ocean temperature (0-200m depth) was found to be higher than the simulated sea surface temperature in the Barents Sea. Smedsrud et al. (2013) also showed that there were strong correlations between the sea ice cover in the Barents Sea, the surface air temperatures and inflowing Atlantic water. As a result of the reduced heat transport in the Atlantic water and the lower sea surface temperatures in the Barents Sea in the model, the conditions for the formation of sea ice is better in the simulation and could hence produce higher values for the sea ice extent. A result of colder Atlantic water in the simulation may also contribute to less bottom melting of the sea ice in the Barents Sea and increased sea ice formation, as these processes are closely related to heat transport through the Barents Sea Opening (Sandø et al., 2014).

Figure 4.4 shows that the model simulates the sea ice extent better in March than it does in September, and the interannual variations are also better captured in March, which can be seen by the correlation coefficients (both significant on the 5 % level, see Section 2.3.4). In September, on the other hand, the model seems to simulate both more interannual variability as well as a higher amplitude of these variations. The great trend

in September in the model simulation is likely due to the overestimation of sea ice extent in early years, while the model simulates the sea ice extent better in recent years. This appears to be the reason for the overestimation of the September trend in the simulation compared to what is observed, and the trends in the Barents Sea in Table 3.2 are also likely affected by this, resulting in an overestimation of the summer trend. However, as the sea ice extent in the Barents Sea is approaching ice-free conditions in the observations in the years following 2007, the trend will most likely be greater in winter than in summer. Thus, decreased winter freezing will likely dominate increased summer melting in recent years in the model simulation (as is known from observations). The fact that the model generally simulates the sea ice better in winter, suggests that the model may be lacking some features in the melting process of the sea ice towards summer in the Barents Sea.

The long-term trends are shown as dotted lines through each of the datasets (Figure 4.4). The trends in March are significant on the 5 % level, while the trends in September are not. However, the trend in the simulated sea ice extent in September is significant on the 10 % level. The trend in March is slightly steeper in the observations than for the model data, meaning that the simulated decrease of sea ice in the Barents Sea does not keep up with what is observed. This delayed melting of sea ice in the model was also found by Bentsen et al. (2012), suggesting that the sea ice in the model is not sensitive enough to increased air temperatures as a result of global warming and Arctic amplification (see Figure 1.1). In fact, this is the case for most climate models (e.g., Rampal et al., 2011; Stroeve et al., 2007). Additionally, an underestimation of the sea ice thinning trend is seen, and Winton (2013) suggests that the ice-albedo feedback is too weak in climate models, resulting in an underestimation of the Arctic amplification. An underestimation of the thinning trend will impact the trend in sea ice extent, as thinner ice is easier to melt completely than thicker ice. Actually, most of the models in the CORE-II project underestimated the thinning trend of the sea ice cover by a factor of two, meaning that this underestimation could be due to their common atmospheric forcing (Wang et al., 2016). In most models the coupling between sea ice properties and sea ice drift is weak, and is suggested to be the reason for the underestimation of trends in sea ice area and sea ice thickness in the models (Rampal et al., 2011).

In contrast to winter trends, the trend in sea ice extent in the Barents Sea in September decreases more in the model than in the observations, and the model and the observations also differ most in September. However, note that neither of these trends are statistically significant on the 5 % level. As is shown by Stroeve et al. (2007), the sea ice extent trend for the model mean in 18 IPCC models are also smaller than the observations in the Arctic Ocean, however the mean trend in the models is not as far from observations in March

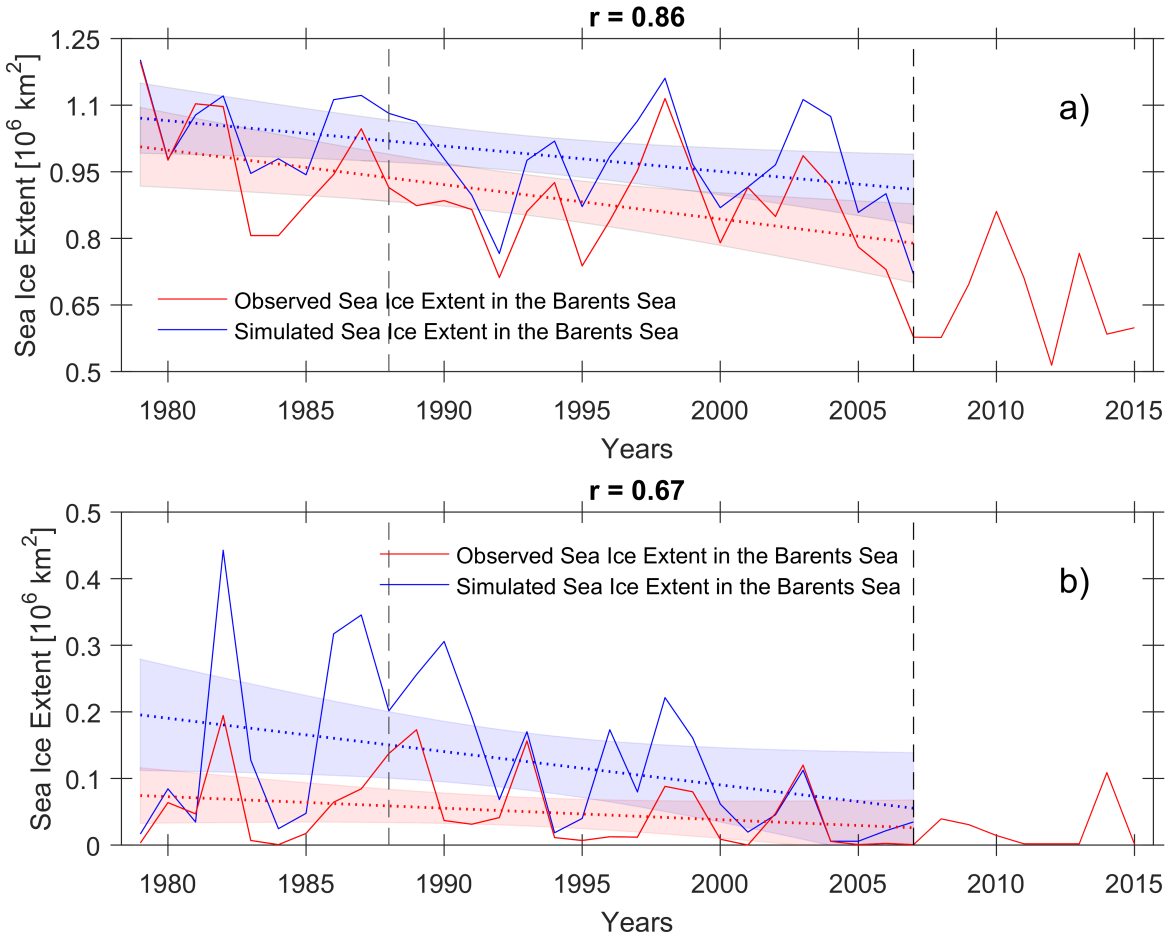

Figure 4.4: *Sea ice extent in the Barents Sea for March (a) and for September (b). The observed sea ice extent (red) is shown for the period 1979-2015 and the simulated sea ice extent (blue) is shown for the period 1979-2007. The dotted lines show the linear trends for the observed (red) and simulated (blue) sea ice extent (1979-2007), and the shaded areas show the 95 % confidence intervals for the linear trend. The vertical dashed lines show Period III (1988-2007) The correlation coefficients for the detrended time series, r, are shown at the top of each panel.*

as it is in September. However, Figure 4.4 only represents the trends in the Barents Sea, where the sea ice cover in September is very small compared to the interior of the Arctic Ocean (e.g., Figure 3.2). Another factor that plays a major role in the melting process of sea ice in the Barents Sea, in addition to the heat transport with the Atlantic water into the Barents Sea, is solar radiation (Sandø et al., 2010).

4.5 Regional and seasonal variations

The Arctic is a vast area, and naturally there are large differences between the various regions within the Arctic Ocean. A big part of this study is to identify and analyze the inter-regional differences in interannual variations and long-term trends, as well as determine whether the different Arctic regions experience an enhanced melting in summer (leading to a reduction of the sea ice extent in September), or a decrease of the refreezing process (leading to a reduction of the sea ice extent in March). The recent decrease of sea ice in the Northern Hemisphere is a result of (at least) one of these two factors, and this thesis aims to find out which one of them is the dominant cause. We note that also wind and ocean currents influence the sea ice loss and regional sea ice variability, as the sea ice can be transported from one region to another. As the sea ice is thinner and more vulnerable in summer, wind and ocean currents possibly contribute more to a larger variability in September than in March. However an analysis of these factors will not be a part of this study.

As mentioned in Section 3.3.2, there are two regions that are seasonally ice-free in the summer time, seven regions that are completely ice-covered during several winter months, and three regions that vary all months of the year. Regions that are ice-free in the summer season do not have a trend in sea ice extent during these summer months (Table 3.2), and will therefore not contribute to the September melting trend during the late summer in the Arctic. Regions that fall into this category are the Bering Sea and the Sea of Okhotsk, which have ice-free conditions four months of the year, from July to October (see Figure 3.4k and 3.4l). The same principle applies to the regions which are completely ice-covered during winter, like the Beaufort Sea, the Chukchi Sea, the East Siberian Sea, the Laptev Sea, the Kara Sea, the Canadian Archipelago and the Central Arctic. These regions do not have a trend in winter months, and will hence not contribute to the trend in sea ice extent in the Northern Hemisphere in March, because they do not have a lack of freezing during winter (since they always reach full coverage of sea ice).

However, the regions with limited months of variability, mentioned in the previous section, can partly contribute to the trends if they clearly start the freeze-up a little later than normally seen (i.e. lack of freezing), or their melting period begins earlier than usual (increased summer melting). In fact, the period of surface melt in the entire Arctic has lengthened by approximately five days per decade over the period from 1979 to 2013 (Stroeve et al., 2014), dominated by later autumn freeze-up between 6 and 11 days per decade within the Kara Sea, the Laptev Sea, the East Siberian Sea, the Chukchi Sea and the Beaufort Sea. This lengthening of the summer season (later freeze-up) supports a

decrease of the refreezing process. In addition to a lengthening of the summer season, a reduction of sea ice concentration in winter is associated with reduced freezing towards the winter. Also, the same applies to a reduction of sea ice thickness in winter. In fact, the sea ice thickness has decreased within the Arctic Basin, resulting in a more vulnerable sea ice cover and a more rapid decrease of sea ice, especially in the summer when the amount of sea ice is lowest and most vulnerable (Haas et al., 2008).

The interannual variations seen in the Northern Hemisphere in September are much larger than the interannual variations seen in March (Figure 3.3), and recent values for the monthly mean sea ice extent (yellow lines) are lower than the mean of the monthly values, and a trend towards lower values of sea ice extent can be seen (especially in the summer months). However, due to the fact that seven of the 12 regions are completely ice-covered in winter, the variations in the Northern Hemisphere are more or less stable in the winter months (see Figure 3.3), since there are only five regions left with a varying sea ice cover in this season. In contrast, only two of the regions are completely ice-free in the summer season, and hence these regions do not contribute to the large variability seen in the same figure in September. The fact that there are less regions with interannual variations in sea ice cover in winter than in summer, can be one of the reasons why the interannual variability seen in March is significantly lower than the variability in September. As a result, this alone does not provide enough evidence that the larger variability in the summer months in the Northern Hemisphere results from enhanced melting in summer rather than decreased melting towards winter.

However, regional trends in sea ice extent in winter (March) and in summer (September) are shown in Table 3.2 over the two periods with the steepest trends in sea ice extent, with respect to the annual mean sea ice extent in the region. This table shows that the largest sea ice loss in total occurs in September, both in Period I and in Period III, as many of the regions are completely ice-covered in March. This in fact supports the discussion in the previous paragraph, and provides a reason to believe that the ongoing melting of the total Arctic sea ice is dominated by enhanced melting in the summer. Negative trends in sea ice extent are found for all months of the year in other studies as well, where the greatest negative trends are also found in the summer season (e.g., Serreze et al., 2007; Parkinson and Cavalieri, 2008; Stroeve et al., 2014). Rigor et al. (2000) showed that Arctic landmasses experienced the greatest warming during spring over the period 1978 to 1997, which may be linked to the fact that the strongest negative trends in sea ice can be seen in September. Higher temperatures in spring contribute to increased sea ice melting in spring and hence a greater loss of sea ice towards summer. As a result, there is more open water able to absorb solar radiation in summer, which is also the season with

the strongest insolation.

Also, Figure 3.5 shows the linear least-square trend line in sea ice concentration in each grid cell, both in summer and winter months. This figure shows that there is a much larger area that experiences a trend in September than in March in Period I, as the trends in March are much more dispersed than they are in September in this period. The trends also appear to be generally greater in September than in March in this period. Furthermore, the trends in Period III appear to be greater than the trends seen in Period I. In Period III practically all regions experience a negative trend in March and there is possibly also a larger area that is affected by a decrease in sea ice concentration than in September. However, the trends in September appear to be greater than the ones seen in March, meaning that the greatest sea ice loss may have occurred in September, except in the Baffin Bay where the trends clearly are greater in March. This is in agreement with the trends in sea ice extent for most of the regions (Table 3.2), which were also found to be greatest in September (except for the Baffin Bay).

Both the atmosphere and the ocean contribute to the melting and non-freezing of sea ice, as previously mentioned in this study. The southernmost regions are most sensitive to incoming warm water. The trends in sea ice extent and sea ice concentration in the winter season are greatest near the sea ice edge, and are seen in the Baffin Bay, the Barents Sea, the Bering Sea and the Greenland Sea. As the temperature in the atmosphere in the Arctic during winter is much colder than the freezing point, and the fact that there is a limited amount of solar radiation in the Arctic during winter, suggests that a decrease of sea ice in these regions during winter is not due to the atmosphere. However, these regions receive relatively warm water from the south, and incoming warm water (especially in the North Atlantic) contributes to reduce the sea ice cover during winter. However, in the Central Arctic there is always available sea ice in winter, and incoming warm Atlantic water in this region results in increased melting during the winter. However, bottom melting occurs in the entire Arctic Ocean during the summer as well (Ivanov et al., 2016). In fact, results from Ivanov et al. (2016) show that the winter melting is due to the incoming warm Atlantic water, and that bottom melting of the sea ice occurs in areas where warm Atlantic water meets the sea ice.

In this study, the trends in sea ice extent in all regions during the last two decades were found to be greater in September than in March, except for the Baffin Bay and for the two regions which have ice-free conditions in the summer season. However, it is known that the recent loss of sea ice in the Barents Sea is in fact due to a lack of freezing during winter. The trends in sea ice concentration in this study over the last two decades supports this

result, while the trends in sea ice extent do not. The trends in sea ice extent show that there is a greater trend in the summer season in the Barents Sea, which is associated with increased summer melting. The reason for this might be due to several reasons, for instance the fact that the model simulation stops in 2007. Also, from Figure 4.4 it is clear that the observed sea ice extent in the Barents Sea experiences an enhanced reduction of the sea ice cover in March in the years after 2007, while a further decrease in September is not possible because the region approaches ice-free conditions. In addition, the simulated sea ice in the Barents Sea in September is also greater than observed (especially in the early years), and during Period III it appears that the simulation approaches the observation towards more recent years. Thus, there is a steep trend from the beginning of Period III to the end of Period III, resulting in a large negative trend in September (Figure 4.4). These factors support that a loss of sea ice in the Barents Sea in the future (and in later observations that exceeds this study period) will be dominated by reduced winter freezing (as is known from later observations), and especially if the Barents Sea becomes permanently ice-free in the summer season.

Since the greatest interannual variability of sea ice extent in the entire Northern Hemisphere occurs in September in NorESM (Figure 3.3) and the greatest trends, both in sea ice extent (Table 3.2) and in sea ice concentration (Figure 3.5) occur in September, it provides a basis to believe that increased melting in spring and early summer (during the melting period) may be the dominating factor in the recent retreat of the Arctic sea ice cover in total. However, there are large inter-regional variations of the sea ice, and the process of increased melting and decreased freezing are closely linked, meaning that a change in one of these processes will clearly affect the other process as well. It is thus not only increased melting during summer that causes the recent sea ice loss, as some regions experience reduced winter freezing. In addition, there are many factors that contribute to the declining sea ice in the Arctic, e.g., the lengthening of the melting period, which affects both increased melting towards summer and decreased freezing towards winter. An increasing melting period during summer leads to increased absorption of solar radiation during summer, and thus directly effects the onset of the freezing process (Stroeve et al., 2014). Results from Perovich et al. (2011) show that the total amount of solar energy absorbed by the ocean may be more sensitive to the timing of melt onset than autumn freeze-up. This can be explained by the larger absorption of short-wave radiation by the ocean, leading to higher sea surface temperatures and a delay of the autumn freeze-up. Because the temperatures in the Arctic are expected to increase in the future, the melting season is also expected to lengthen further (Stroeve et al., 2014).

Chapter 5

Concluding Remarks

In this study, interannual variability and long-term trends in the Arctic sea ice cover were analyzed in a sea ice-ocean hindcast simulation, and the simulation was supported by observations. The Norwegian Earth System Model (NorESM) was used, forced with atmospheric reanalysis data from the Coordinated Ocean-ice Reference Experiments phase II (CORE-II) project, spanning the 60-year period from 1948 to 2007. In addition, observations were used for comparison and evaluation of the model data from 1979 to 2007. Regional and seasonal trends in the sea ice cover, as well as interannual variability, were the focus in this study.

The model simulation of sea ice extent was found to be realistic compared to the observations that were used in this study (Figure 1.2). Especially, the model captured a similar interannual variability as in the observations. However, even though there were seasonal variations, the mean state of the sea ice cover was underestimated in total in the model simulation. In addition, the results were found to be consistent with existing regional studies of long-term trends, which shows that the sea ice cover rapidly retreated in the last three decades (1979-2006), with a loss of about $-45 \cdot 10^3$ km^2 sea ice per year in the Northern Hemisphere (Parkinson and Cavalieri, 2008). It was shown that during the last 20 years the Arctic sea ice concentration has decreased both in the summer season as well as in the winter season, and in all of the Arctic regions (Figure 3.5). However, the regional rate of decrease largely depends on the geographical location, as the location largely determines the seasonal variations of the sea ice cover.

The first two decades in the model data, Period I (1948-1967), and the last two decades in the model data, Period III (1988-2007), were found to have large positive and negative trends in sea ice extent in the Northern Hemisphere, respectively (Figure 1.2). This was also seen for the Barents Sea. Available observations from this region were used, and the large variability of the sea ice cover during these periods was found to be highly linked

to changes in both air and ocean temperatures. The increase of sea ice extent in Period I was linked to the relatively low air temperatures in the area in this period (Figure 4.2), while the decrease of sea ice extent in Period III was linked to ongoing global warming, which is also amplified in the Arctic region. Increasing ocean temperatures in the model were also found to have great impact on the loss of sea ice in the Barents Sea (Figure 4.3). In addition, not only have the ocean temperatures increased, but an increased heat transport into the Barents Sea has been seen as well (Årthun et al., 2012).

Regional and seasonal differences in sea ice were found, both in interannual variability and long-term trends. It was found that seven of the regions with a full sea ice cover in winter did not have a trend in sea ice extent in March (Table 3.2). These regions are located in the interior of the Arctic (Figure 1.3), and covers the Beaufort Sea, the Chukchi Sea, the East Siberian Sea, the Laptev Sea, the Kara Sea, the Canadian Archipelago and the Central Arctic. As these regions have the strongest negative trend in sea ice in the summer season (hence reduced sea ice cover in summer), it was argued that the loss of sea ice in these regions were associated with increased summer melting. On the other hand, a stronger negative trend in winter (and hence a reduction of the winter sea ice cover) was associated with reduced freezing in the winter season. Two of 12 regions are ice-free in the summer season, and hence these two regions do not have a change in sea ice extent in the summer season. As a result, the winter trend is greater and hence the retreating sea ice in the Bering Sea and the Sea of Okhotsk was associated with decreased freezing of sea ice towards winter. The three remaining regions are the Barents Sea, the Greenland Sea and the Baffin Bay, which vary all months of the year. The Baffin Bay clearly has a stronger winter trend in sea ice concentration and in sea ice extent, meaning that decreased winter freezing is likely the dominant cause of sea ice loss in this region. The Greenland Sea experienced trends on the same order of magnitude both in the summer and in winter, and in the Barents Sea the trends in sea ice concentration and the sea ice extent were contradictory. Due to the fact that the September sea ice extent approaches zero in recent observations in these two latter regions, it was discussed that even though the sea ice extent appears to be dominated by increased summer melting in the model simulation, decreased melting towards winter will likely be the dominant cause of sea ice loss in these regions in the future.

For the Northern Hemisphere in total, the trends seen in summer are stronger than the ones seen in the winter season, both in sea ice extent and in sea ice concentration, and the largest interannual variability was found in summer Figure 3.3. This suggests that NorESM, forced with the atmospheric state from CORE-II, are dominated by a diminishing sea ice cover as a result of increased melting in this study period (1948-2007).

However, as the Arctic is approaching ice-free conditions in the summer season, it gives a reason to believe that the loss of sea ice due to decreased freezing towards the winter season will be more important in the future. We note that a prolonging of the melting season may affect both increased melting towards summer and decreased freezing towards winter, and that wind and ocean currents impact the sea ice drift.

Based on this study, a further model analysis of the Arctic sea ice cover could be carried out. For instance, sea ice drift has a large impact on the interannual variability in different regions. In addition, a study of wind and ocean currents could be carried out to get a better understanding of the sea ice cover. The study could also be expanded to calculate the long-term trends in all months of the year to get a more detailed description of the seasonality of the Arctic sea ice cover. The melting period could be studied further, to see if there has been a significant lengthening of the melting period recently, and if this lengthening occurs mostly in spring or in autumn. The sea ice thickness and the sea ice age can also be taken into account in a further study, as a reduction of these quantities will be important in the future, since they explain much of the rapid decline of the sea ice cover which has been seen recently.

Bibliography

Årthun, M., Eldevik, T., Smedsrud, L. H., Skagseth, O., and Ingvaldsen, R. B. (2012). Quantifying the Influence of Atlantic Heat on Barents Sea Ice Variability and Retreat. *Journal of Climate*, 25(13):4736–4743. http://dx.doi.org/10.1175/JCLI-D-11-00466.1.

Bentsen, M., Bethke, I., Debernard, J., Iversen, T., Kirkevåg, A., Seland, Ø., Drange, H., Roelandt, C., Seierstad, I., Hoose, C., et al. (2012). The Norwegian Earth System Model, NorESM1-M-Part 1: Description and basic evaluation of the physical climate. *Geoscientific Model Development Discussions*, 5:2843–2931. http://dx.doi.org/10.5194/gmdd-5-2843-2012.

Bjørnstad, J. (2009). *Frihetsgrad: Statistikk*. Store norske leksikon. Retrieved from https://snl.no/frihetsgrad/statistikk. Accessed 02.04.2016.

Bleck, R. and Smith, L. T. (1990). A wind-driven isopycnic coordinate model of the north and equatorial Atlantic Ocean: 1. Model development and supporting experiments. *Journal of Geophysical Research: Oceans*, 95(C3):3273–3285. http://dx.doi.org/10.1029/JC095iC03p03273.

Cavalieri, D. J. and Parkinson, C. L. (2012). Arctic sea ice variability and trends, 1979-2010. *Cryosphere*, 6(4):881–889. http://dx.doi.org/10.5194/tc-6-881-2012.

Cavalieri, D. J., Parkinson, C. L., Gloersen, P., and Zwally, H. J. (1996). Updated yearly. *Sea Ice Concentrations from Nimbus-7 SMMR and DMSP SSM/I-SSMIS Passive Microwave Data, Version 1.*.Boulder, Colorado USA. NASA National Snow and Ice Data Center Distributed Active Archive Center. Retrieved from http://dx.doi.org/10.5067/8GQ8LZQVL0VL. Accessed 30.11.2015.

Close, S., Houssais, M.-N., and Herbaut, C. (2015). Regional dependence in the timing of onset of rapid decline in Arctic sea ice concentration. *Journal of Geophysical Research: Oceans*, 120(12):8077–8098. http://dx.doi.org/10.1002/2015JC011187.

Comiso, J. C. (2002). A rapidly declining perennial sea ice cover in the Arctic. *Geophysical Research Letters*, 29(20):17–1–17–4. http://dx.doi.org/10.1029/2002GL015650.

Danabasoglu, G., Yeager, S. G., Bailey, D., Behrens, E., Bentsen, M., Bi, D., Biastoch, A., Boening, C., Bozec, A., Canuto, V. M., Cassou, C., Chassignet, E., Coward, A. C., Danilov, S., Diansky, N., Drange, H., Farneti, R., Fernandez, E., Fogli, P. G., Forget, G., Fujii, Y., Griffies, S. M., Gusev, A., Heimbach, P., Howard, A., Jung, T., Kelley, M., Large, W. G., Leboissetier, A., Lu, J., Madec, G., Marsland, S. J., Masina, S., Navarra, A., Nurser, A. J. G., Pirani, A., Salas y Melia, D., Samuels, B. L., Scheinert, M., Sidorenko, D., Treguier, A.-M., Tsujino, H., Uotila, P., Valcke, S., Voldoire, A., and Wangi, Q. (2014). North Atlantic simulations in Coordinated Ocean-ice Reference Experiments phase II (CORE-II). Part I: Mean states. *Ocean Modelling*, 73:76–107. http://dx.doi.org/10.1016/j.ocemod.2013.10.005.

Dobricic, S., Vignati, E., and Russo, S. (2016). Large-Scale Atmospheric Warming in Winter and the Arctic Sea Ice Retreat. *Journal of Climate*, 29(8):2869–2888. http://dx.doi.org/10.1175/JCLI-D-15-0417.1.

Fetterer, F., Savoie, M., Helfrich, S., and Clemente-Colon, P. (2010). Updated daily. National Ice Center and National Snow and Ice Data Center. *Multisensor Analyzed Sea Ice Extent - Northern Hemisphere (MASIE-NH), Version 1.*Boulder, Colorado USA. NSIDC: National Snow and Ice Data Center. Retrieved from http://dx.doi.org/10.7265/N5GT5K3K. Accessed 29.08.2015.

Førland, E. J., Benestad, R., Hanssen-Bauer, I., Haugen, J. E., and Skaugen, T. E. (2012). Temperature and precipitation development at Svalbard 1900–2100. *Advances in Meteorology*, 2011. http://dx.doi.org/10.1155/2011/893790.

Griffies, S. M., Biastoch, A., Boening, C., Bryan, F., Danabasoglu, G., Chassignet, E. P., England, M. H., Gerdes, R., Haak, H., Hallberg, R. W., Hazeleger, W., Jungclaus, J., Large, W. G., Madec, G., Pirani, A., Samuels, B. L., Scheinert, M., Sen Gupta, A., Severijns, C. A., Simmons, H. L., Treguier, A. M., Winton, M., Yeager, S., and Yin, J. (2009). Coordinated Ocean-ice Reference Experiments (COREs). *Ocean Modelling*, 26(1-2):1–46. http://dx.doi.org/10.1016/j.ocemod.2008.08.007.

Griffies, S. M., Yin, J., Durack, P. J., Goddard, P., Bates, S. C., Behrens, E., Bentsen, M., Bi, D., Biastoch, A., Boening, C. W., Bozec, A., Chassignet, E., Danabasoglu, G., Danilov, S., Domingues, C. M., Drange, H., Farneti, R., Fernandez, E., Greatbatch, R. J., Holland, D. M., Ilicak, M., Large, W. G., Lorbacher, K., Lu, J., Marsland, S. J., Mishra, A., Nurser, A. J. G., Salas y Melia, D., Palter, J. B., Samuels, B. L., Schroeter, J., Schwarzkopf, F. U., Sidorenko, D., Treguier, A. M., Tseng, Y.-h., Tsujino, H., Uotila, P., Valcke, S., Voldoire, A., Wang, Q., Winton, M., and

Zhang, X. (2014). An assessment of global and regional sea level for years 1993-2007 in a suite of interannual CORE-II simulations. *Ocean Modelling*, 78:35–89. http://dx.doi.org/10.1016/j.ocemod.2014.03.004.

Haas, C., Pfaffling, A., Hendricks, S., Rabenstein, L., Etienne, J.-L., and Rigor, I. (2008). Reduced ice thickness in Arctic Transpolar Drift favors rapid ice retreat. *Geophysical Research Letters*, 35(17). http://dx.doi.org/10.1029/2008GL034457.

Hartmann, D., Klein Tank, A., Rusticucci, M., Alexander, L., Bronnimann, S., Charabi, Y., Dentener, F., Dlugokencky, E., Easterling, D., Kaplan, A., Soden, B., Thorne, P., Wild, M., and Zhai, P., editors (2013). *Observations: Atmosphere and Surface. In Climate Change 2013: The Physical Science Basis. Contribution of Working Group I to the Fifth Assessment Report of the Intergovernmental Panel on Climate Change (IPCC)*, Book Section 2, pages 159–254. [Stocker, T.F. and Qin, D. and Plattner, G.-K. and Tignor, M. and Allen, S.K. and Boschung, J. and Nauels, A. and Xia, Y. and Bex, V. and Midgley, P.M.]. Cambridge University Press, Cambridge, United Kingdom and New York, NY, USA. www.climatechange2013.org.

Hogg, R. V. and Tanis, E. A. (2010). *Probability and Statistical Inference*. Pearson Education, Upple Saddle River, New Jersey, 8 edition.

Hogg, R. V., Tanis, E. A., and Zimmerman, D. L. (2014). *Probability and Statistical Inference*. Pearson Education, Boston, 9 edition.

Holloway, J. L. (1958). Smoothing and filtering of time series and space fields. *Advances in geophysics*, 4:351–389.

Hunke, E. C., Lipscomb, W. H., Turner, A. K., et al. (2010). CICE: the Los Alamo's Sea Ice Model Documentation and Software User's Manual Version 4.1 LA-CC-06-012. *T-3 Fluid Dynamics Group, Los Alamos National Laboratory*, 675.

Ilicak, M., Drange, H., Wang, Q., Gerdes, R., Aksenov, Y., Bailey, D., Bentsen, M., Biastoch, A., Bozec, A., Boning, C., Cassou, C., Chassignet, E., Coward, A. C., Curry, B., Danabasoglu, G., Danilov, S., Fernandez, E., Fogli, P. G., Fujii, Y., Griffies, S. M., Iovino, D., Jahn, A., Jung, T., Large, W. G., Lee, C., Lique, C., Lu, J., Masina, S., Nurser, A. G., Roth, C., y Melia, D. S., Samuels, B. L., Spence, P., Tsujino, H., Valcke, S., Voldoire, A., Wang, X., and Yeager, S. G. (2016). An assessment of the Arctic Ocean in a suite of interannual CORE-II simulations. Part III: Hydrography and fluxes. *Ocean Modelling*, 100:141 – 161. http://dx.doi.org/10.1016/j.ocemod.2016.02.004.

IPCC (2013). *Summary for Policymakers. In Climate Change 2013: The Physical Science Basis. Contribution of Working Group I to the Fifth Assessment Report of the*

Intergovernmental Panel on Climate Change (IPCC), Book Section SPM, pages 1–30. [Stocker, T.F. and Qin, D. and Plattner, G.-K. and Tignor, M. and Allen, S.K. and Boschung, J. and Nauels, A. and Xia, Y. and Bex, V. and Midgley, P.M.]. Cambridge University Press, Cambridge, United Kingdom and New York, NY, USA. www.climatechange2013.org.

Ivanov, V., Alexeev, V., Koldunov, N. V., Repina, I., Sandø, A. B., Smedsrud, L. H., and Smirnov, A. (2016). Arctic Ocean Heat Impact on Regional Ice Decay: A Suggested Positive Feedback. *Journal of Physical Oceanography*, 46(5):1437–1456. http://dx.doi.org/10.1175/JPO-D-15-0144.1.

Janson, L., Fithian, W., and Hastie, T. J. (2015). Effective Degrees of Freedom: A Flawed Metaphor. *Biometrika*, 102(2):479–485. http://dx.doi.org/10.1093/biomet/asv019.

Kimura, R. (2002). Numerical weather prediction. *Journal of Wind Engineering and Industrial Aerodynamics*, 90(12–15):1403 – 1414. http://dx.doi.org/10.1016/S0167-6105(02)00261-1.

Koenigk, T., Brodeau, L., Graversen, R. G., Karlsson, J., Svensson, G., Tjernström, M., Willén, U., and Wyser, K. (2013). Arctic climate change in 21st century CMIP5 simulations with EC-Earth. *Climate Dynamics*, 40(11):2719–2743. http://dx.doi.org/10.1007/s00382-012-1505-y.

Kvingedal, B. (2005). *Sea-Ice Extent and Variability in the Nordic Seas, 1967-2002*, pages 39–49. American Geophysical Union. http://dx.doi.org/10.1029/158GM04.

Kwok, R., Cunningham, G. F., Wensnahan, M., Rigor, I., Zwally, H. J., and Yi, D. (2009). Thinning and volume loss of the Arctic Ocean sea ice cover: 2003-2008. *Journal of Geophysical Research: Oceans*, 114(C7). http://dx.doi.org/10.1029/2009JC005312.

Large, W. G. and Yeager, S. G. (2009). The global climatology of an interannually varying air–sea flux data set. *Climate Dynamics*, 33(2):341–364. http://dx.doi.org/10.1007/s00382-008-0441-3.

Manabe, S. and Wetherald, R. T. (1975). The effects of doubling the CO2 concentration on the climate of a general circulation modell. *Journal of the Atmospheric Sciences*, 3:3–15.

Mason, J. (1986). Numerical Weather Prediction. *Proceedings of the Royal Society of London Series A*, 407:51–60. http://dx.doi.org/10.1098/rspa.1986.0083.

Montgomery, D. C., Peck, E. A., and Vining, G. G. (2015). *Introduction to Linear Regression Analysis*. John Wiley & Sons, Hoboken, New Jersey, 5 edition.

O'Haver, T. (1997). A Pragmatic Introduction to Signal Processing. Retrieved from https://terpconnect.umd.edu/~toh/spectrum/IntroToSignalProcessing.pdf. Accessed 28.04.2016.

Onarheim, I. H., Smedsrud, L. H., Ingvaldsen, R. B., and Nilsen, F. (2014). Loss of sea ice during winter north of Svalbard. *Tellus A*, 66. http://dx.doi.org/10.3402/tellusa.v66.23933.

Overland, J. E. and Wang, M. (2007). Future regional Arctic sea ice declines. *Geophysical Research Letters*, 34(17). http://dx.doi.org/10.1029/2007GL030808.

Overland, J. E. and Wang, M. (2010). Large-scale atmospheric circulation changes are associated with the recent loss of Arctic sea ice. *Tellus A*, 62(1):1–9. http://dx.doi.org/10.1111/j.1600-0870.2009.00421.x.

Parkinson, C. L. and Cavalieri, D. J. (2008). Arctic sea ice variability and trends, 1979-2006. *Journal of Geophysical Research: Oceans*, 113(C7). http://dx.doi.org/10.1029/2007JC004558.

Perovich, D., Jones, K., Light, B., Eicken, H., Markus, T., Stroeve, J., and Lindsay, R. (2011). Solar partitioning in a changing Arctic sea-ice cover. *Annals of Glaciology*, 52(57):192–196. http://dx.doi.org/10.3189/172756411795931543.

Petoukhov, V. and Semenov, V. A. (2010). A link between reduced Barents-Kara sea ice and cold winter extremes over northern continents. *Journal of Geophysical Research: Atmospheres*, 115(D21). http://dx.doi.org/10.1029/2009JD013568.

Pielke, R. A. (2013). *Mesoscale Meteorological Modeling*, volume 98. Elsevier, Academic press, Amsterdam, 3 edition.

Quenouille, M. H. et al. (1952). *Associated measurements*. Butterworths Scientific Publications, London, UK. page 242.

Rampal, P., Weiss, J., Dubois, C., and Campin, J.-M. (2011). IPCC climate models do not capture Arctic sea ice drift acceleration: Consequences in terms of projected sea ice thinning and decline. *Journal of Geophysical Research: Oceans*, 116(C8). http://dx.doi.org/10.1029/2011JC007110.

Rigor, I. G., Colony, R. L., and Martin, S. (2000). Variations in Surface Air Temperature Observations in the Arctic, 1979-97. *Journal of Climate*, 13(5):896–914. http://dx.doi.org/10.1175/1520-0442(2000)013¡0896:VISATO¿2.0.CO;2.

Rigor, I. G. and Wallace, J. M. (2004). Variations in the age of Arctic sea-ice and summer sea-ice extent. *Geophysical Research Letters*, 31(9). http://dx.doi.org/10.1029/2004GL019492.

Rosenzweig, C., Iglesias, A., Yang, X., Epstein, P. R., and Chivian, E. (2001). Climate change and extreme weather events; implications for food production, plant diseases, and pests. *Global Change and Human Health*, 2(2):90–104. http://dx.doi.org/10.1023/A:1015086831467.

Sandø, A. B., Gao, Y., and Langehaug, H. R. (2014). Poleward ocean heat transports, sea ice processes, and Arctic sea ice variability in NorESM1-M simulations. *Journal of Geophysical Research: Oceans*, 119(3):2095–2108. http://dx.doi.org/10.1002/2013JC009435.

Sandø, A. B., Nilsen, J. E. Ø., Gao, Y., and Lohmann, K. (2010). Importance of heat transport and local air-sea heat fluxes for Barents Sea climate variability. *Journal of Geophysical Research: Oceans*, 115(C7). http://dx.doi.org/10.1029/2009JC005884.

Serreze, M. C. and Barry, R. G. (2011). Processes and impacts of Arctic amplification: A research synthesis. *Global and Planetary Change*, 77(1-2):85 – 96. http://dx.doi.org/10.1016/j.gloplacha.2011.03.004.

Serreze, M. C. and Francis, J. A. (2006). The Arctic Amplification Debate. *Climatic Change*, 76(3):241–264. http://dx.doi.org/10.1007/s10584-005-9017-y.

Serreze, M. C., Holland, M. M., and Stroeve, J. (2007). Perspectives on the Arctic's Shrinking Sea-Ice Cover. *Science*, 315(5818):1533–1536. http://dx.doi.org/10.1126/science.1139426.

Smedsrud, L. H., Esau, I., Ingvaldsen, R. B., Eldevik, T., Haugan, P. M., Li, C., Lien, V. S., Olsen, A., Omar, A. M., Otterå, O. H., et al. (2013). The role of the Barents Sea in the Arctic climate system. *Reviews of Geophysics*, 51(3):415–449. http://dx.doi.org/10.1002/rog.20017.

Stocker, T., Qin, D., Plattner, G.-K., Alexander, L., Allen, S., Bindoff, N., Breon, F.-M., Church, J., Cubasch, U., Emori, S., Forster, P., Friedlingstein, P., Gillett, N., Gregory, J., Hartmann, D., Jansen, E., Kirtman, B., Knutti, R., Krishna Kumar, K., Lemke, P., Marotzke, J., Masson-Delmotte, V., Meehl, G., Mokhov, I., Piao, S., Ramaswamy, V., Randall, D., Rhein, M., Rojas, M., Sabine, C., Shindell, D., Talley, L., Vaughan, D., and Xie, S.-P., editors (2013). *Technical Summary. In Climate Change 2013: The Physical Science Basis. Contribution of Working Group I to the Fifth Assessment Report*

of the Intergovernmental Panel on Climate Change (IPCC), Book Section TS, pages 33–115. [Stocker, T.F. and Qin, D. and Plattner, G.-K. and Tignor, M. and Allen, S.K. and Boschung, J. and Nauels, A. and Xia, Y. and Bex, V. and Midgley, P.M.]. Cambridge University Press, Cambridge, United Kingdom and New York, NY, USA. www.climatechange2013.org.

Stroeve, J., Holland, M. M., Meier, W., Scambos, T., and Serreze, M. (2007). Arctic sea ice decline: Faster than forecast. *Geophysical Research Letters*, 34(9). http://dx.doi.org/10.1029/2007GL029703.

Stroeve, J. C., Markus, T., Boisvert, L., Miller, J., and Barrett, A. (2014). Changes in Arctic melt season and implications for sea ice loss. *Geophysical Research Letters*, 41(4):1216–1225. http://dx.doi.org/10.1002/2013GL058951.

Taylor, P. C., Cai, M., Hu, A., Meehl, J., Washington, W., and Zhang, G. J. (2013). A Decomposition of Feedback Contributions to Polar Warming Amplification. *Journal of Climate*, 26(18):7023–7043. http://dx.doi.org/10.1175/JCLI-D-12-00696.1.

Vaughan, D., Comiso, J., Allison, I., Carrasco, J., Kaser, G., Kwok, R., Mote, P., Murray, T., Paul, F., Ren, J., Rignot, E., Solomina, O., Steffen, K., and Zhang, T., editors (2013). *Observations: Cryosphere. In Climate Change 2013: The Physical Science Basis. Contribution of Working Group I to the Fifth Assessment Report of the Intergovernmental Panel on Climate Change (IPCC)*, Book Section TS, pages 317–382. [Stocker, T.F. and Qin, D. and Plattner, G.-K. and Tignor, M. and Allen, S.K. and Boschung, J. and Nauels, A. and Xia, Y. and Bex, V. and Midgley, P.M.]. Cambridge University Press, Cambridge, United Kingdom and New York, NY, USA. www.climatechange2013.org.

Vihma, T. (2014). Effects of Arctic sea ice decline on weather and climate: A review. *Surveys in Geophysics*, 35(5):1175–1214. http://dx.doi.org/10.1007/s10712-014-9284-0.

Wang, Q., Ilicak, M., Gerdes, R., Drange, H., Aksenov, Y., Bailey, D. A., Bentsen, M., Biastoch, A., Bozec, A., Böning, C., et al. (2016). An assessment of the Arctic Ocean in a suite of interannual CORE-II simulations. Part I: Sea ice and solid freshwater. *Ocean Modelling*. http://dx.doi.org/10.1016/j.ocemod.2015.12.008.

Winton, M. (2013). *Sea Ice–Albedo Feedback and Nonlinear Arctic Climate Change*, pages 111–131. American Geophysical Union. http://dx.doi.org/10.1029/180GM09.

Woodgate, R. A., Aagaard, K., and Weingartner, T. J. (2006). Interannual changes in the Bering Strait fluxes of volume, heat and freshwater between 1991 and 2004. *Geophysical Research Letters*, 33(15). http://dx.doi.org/10.1029/2006GL026931.